



Forschungszentrum Karlsruhe
in der Helmholtz-Gemeinschaft

Wissenschaftliche Berichte
FZKA 7424

Magnetohydrodynamic Flow in a Mock-Up of a HCLL Blanket Part II Experiments

**L. Bühler, H.-J. Brinkmann, S. Horanyi,
K. Starke**

**Institut für Kern- und Energietechnik
Programm Kernfusion**

September 2008

Forschungszentrum Karlsruhe

in der Helmholtz Gemeinschaft

Wissenschaftliche Berichte

FZKA 7424

**Magnetohydrodynamic flow
in a mock-up of a HCLL blanket
Part II Experiments**

L. Bühler, H.-J. Brinkmann, S. Horanyi, K. Starke

Institut für Kern- und Energietechnik
Programm Kernfusion

Forschungszentrum Karlsruhe GmbH, Karlsruhe
2008

Für diesen Bericht behalten wir uns alle Rechte vor

Forschungszentrum Karlsruhe GmbH
Postfach 3640, 76021 Karlsruhe

Mitglied der Hermann von Helmholtz-Gemeinschaft
Deutscher Forschungszentren (HGF)

ISSN 0947-8620

urn:nbn:de:0005-074249

Magnetohydrodynamic flow in a mock-up of a HCLL blanket

Part II Experiments in a uniform magnetic field

Abstract

Liquid-metal magnetohydrodynamic flows in a scaled mock-up of a helium cooled lead lithium test blanket module for ITER have been investigated experimentally in order to provide a data base as support of the proposed design concept and for validation of numerical tools. The experimental mock-up has been built according to the design developed at CEA as a European candidate for a liquid-metal test blanket module in ITER (Rampal, Li-Puma, Poitevin, Rigal, Szczepanski and Boudot (2005)). In this concept the eutectic liquid-metal alloy PbLi serves as breeder material while the entire thermal power released in the blanket is removed by helium that flows at high pressure and velocity inside small channels embedded in walls and cooling plates. The original geometry is scaled down by a factor of 2 to fit into the large magnet available in the MEKKA laboratory of the Forschungszentrum Karlsruhe, where NaK is used as a model fluid. Measurements of pressure and potential distribution on the surface of the mock-up have been performed for various combinations of magnetic field strengths and flow rates, quantified by the relevant nondimensional groups, the Hartmann number Ha and the Reynolds number Re , respectively.

The experiments confirm previous theoretical predictions that the major part of pressure drop appears in the entrance and exit pipes and in poloidal manifolds. Additional but smaller contributions are present when the flow passes through the narrow gaps in the back plate or at the first wall. The pressure drop in breeder units, where velocities of the order of 1 – 2 mm/s are foreseen, is negligible in comparison with the other contributions. The large range of investigated parameters such as $500 \leq Ha \leq 5000$, $200 < Re < 10000$ allows defining a general pressure drop correlation to be used for extrapolations of results to ITER or DEMO conditions.

Results for electric potential measurements on the surface of the module yield information about flow distribution between the cooling plates. For strong magnetic fields and moderate flow rates the agreement with numerical predictions seems quite satisfactory considering the very complicated geometry for which calculations in a central cross section have been performed taking into account the full electromagnetic coupling. A strong coupling results in sufficiently uniform flow distribution in breeder units with increased flow in lateral sub-channels along the so-called grid plates. Inertia effects become more expressed for smaller magnetic fields and higher flow rates. For such conditions at lower Hartmann numbers Ha and larger Reynolds numbers Re the flow distributions in breeder units become non-symmetric and regions with even reversed flow could appear, forming closed recirculation loops in breeder units.

Magnetohydrodynamische Strömungen im Modellexperiment eines HCLL Blankets

Teil II Experimente in einem homogenen Magnetfeld

Zusammenfassung

In einem skalierten Modell eines Helium-gekühlten Blei-Lithium Testblanketmoduls für ITER wurden magnetohydrodynamische Flüssigmetall-Strömungen untersucht. Die Ergebnisse untermauern das untersuchte Designkonzept und dienen zur Validierung von numerischen Berechnungsverfahren. Die untersuchte Modellgeometrie wurde entsprechend einem bei der CEA entwickelten Design eines Europäischen Konzepts eines Flüssigmetall-Blankets für ITER gefertigt (Rampal et al. (2005)). In diesem Entwurf dient die eutektische Flüssigmetalllegierung PbLi als Brutmaterial. Die im Blanket freigesetzte thermische Leistung wird durch Helium abgeführt, das bei hohen Drücken und Geschwindigkeiten in engen Kanälen innerhalb der Wände und in Kühlplatten strömt. Die Originalgeometrie wurde um einen Faktor 2 verkleinert, damit das Experiment im großen Magneten des MEKKA Labors im Forschungszentrum Karlsruhe Platz findet, wo NaK als Modellfluid eingesetzt wird. Auf der Oberfläche des Modells wurden Druck- und Potentialverteilungen für eine Vielzahl von Parameterkombinationen gemessen. Als dimensionslose Größen zur Quantifizierung der Magnetfeldstärke und des Volumenstroms dienen die Hartmann - Zahl Ha und die Reynolds - Zahl Re .

Die experimentellen Ergebnisse bestätigen theoretische Vorhersagen, wonach die größten Druckverluste in den Zu- und Abflussleitungen und in den poloidalen Verteilern und Sammlern entstehen. Zusätzliche kleinere Beiträge ergeben sich, wenn die Strömung durch schmale Öffnungen in der Rückwand und nahe der ersten Wand hindurch tritt. Im Vergleich mit diesen Anteilen ist der Druckverlust in den Bruteinheiten bei Strömungsgeschwindigkeiten von 1 – 2 mm/s vernachlässigbar klein. Aus dem weiten Bereich der untersuchten Parameter, $500 \leq Ha \leq 5000$, $200 < Re < 10000$, kann eine Druckverlust-Korrelation abgeleitet werden, mit deren Hilfe die Ergebnisse auf ITER oder DEMO Bedingungen extrapoliert werden können.

Aus Messungen des elektrischen Potentials auf der Oberfläche des Moduls kann die Strömungsverteilung zwischen den Kühlplatten ermittelt werden. Trotz der komplexen Geometrie findet man für starke Magnetfelder und moderate Volumenströme eine recht gute Übereinstimmung mit Ergebnissen numerischer Berechnungen, die die volle elektrische Kopplung zwischen Unterkanälen und Bruteinheiten für eingelaufene Bedingungen in einer Mittelebene des Blankets berücksichtigen. Die starke elektromagnetische Kopplung führt zu einer hinreichend gleichförmigen Strömungsverteilung innerhalb der Bruteinheiten, mit etwas erhöhten Durchsätzen in den äußeren Kanälen entlang den sogenannten Grid Plates. Trägheitseffekte treten verstärkt bei schwächeren Magnetfeldern oder höheren Strömungsgeschwindigkeiten in Erscheinung. Für solche Bedingungen, bei kleineren Hartmann - Zahlen Ha und großen Reynolds - Zahlen Re , wird die Strömungsverteilung in den Bruteinheiten unsymmetrisch und es entstehen Gebiete mit Rückströmung oder geschlossene Rezirkulationsgebiete.

Magnetohydrodynamic flow in a mock-up of a HCLL blanket

Part II Experiments in a uniform magnetic field

Contents

1	Introduction	1
2	Flow conditions in a HCLL blanket	5
3	Test section	8
3.1	Design of the MHD mock-up of an ITER TBM	8
3.2	Fabrication	8
3.3	Wetting procedure	12
4	The MEKKA laboratory	15
4.1	Liquid metal loop	15
4.2	Magnetic field	18
4.3	Flow rate measurements	18
4.4	Pressure difference measurements	20
4.5	Surface potential measurements	23
4.6	Data acquisition	28
5	Results	29
5.1	Pressure measurements	29
5.2	Potential measurements	37
5.3	Flow distribution	42
5.4	Extrapolation to ITER TBM conditions	47
6	Conclusions	50
	References	53
A	Appendix	55

1 Introduction

The *Helium-Cooled Lead Lithium* (HCLL) blanket is a promising candidate for a breeding blanket in a future fusion power reactor, where the eutectic alloy PbLi is considered as a liquid breeder material for generation of tritium that is one of the fuel components. The design of this blanket concept is guided by the idea of using low velocities in the box-shaped breeder units required for tritium extraction from the blanket and for purification of the liquid metal. The heat is removed in this type of blanket by pure thermal conductance through helium cooled walls. It is expected that the small velocities (1 – 2 mm/s) reduce the *magnetohydrodynamic* (MHD) effects and keep the pressure drop at acceptable values even if no electrical insulation is foreseen on the walls. This fact allows the fabrication of the blanket from available material using standard fabrication techniques and it makes the HCLL blanket become the European candidates for a liquid metal *Test Blanket Module* (TBM) in ITER (Rampal et al. (2005), Rampal, Gatelet, Giancarli, Laffont, Li-Puma, Salavy and Rigal (2006)). A HCLL blanket is based on a modular design, where a large number of so-called *Breeder Units* (BU) is arranged in an array and combined to a blanket module as shown in Fig. 1. In such a modular blanket each column of BUs is fed with liquid metal through a poloidal manifold. Details of a single BU are displayed in Fig. 2, and Fig. 3 shows the poloidal manifold for a DEMO blanket module supplying 8 breeder units. These latter ones are hydraulically connected at the first wall where the fluid passes through a thin gap into other 8 units which are drained by a similar manifold. For applications in DEMO reactor one column consists of 16 BUs while the TBM for ITER has only 8 units in each poloidal column.

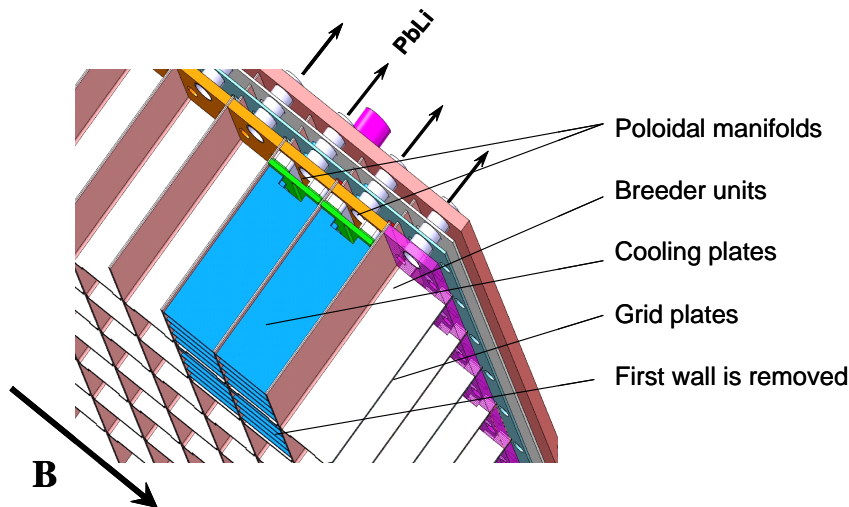


Figure 1: CEA design of a HCLL blanket module with box-shaped breeder units filled with liquid metal. The heat is removed by 5 cooling plates inserted in each unit.

Although the MHD effects in single HCLL blanket boxes seem to play a minor role at the first view it is necessary to investigate a number of issues prior to an application in such a complex system like ITER to ensure entire functionality, reliability, and safety of the test blanket module. While in the breeder units the velocities and perhaps the MHD pressure drop remains acceptably small, velocities in the piping system are still considerable, since a large

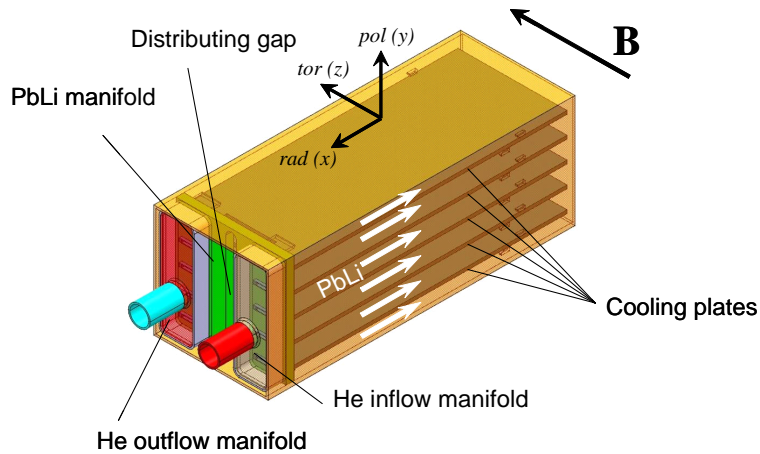


Figure 2: View on a single breeder unit with cooling plates. The fluid enters the BU through the narrow gap in the (green) back plate.

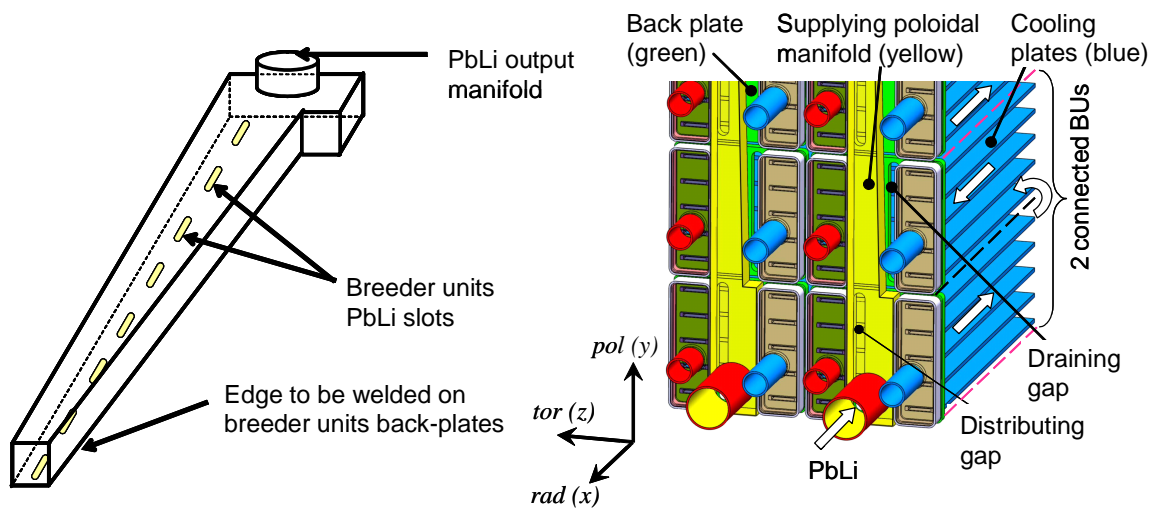


Figure 3: Details of the poloidal manifold for a DEMO blanket module. The liquid metal enters the poloidal manifold (yellow) through the circular access tube, flows along the poloidal manifold, and enters the BU through a narrow gap or slot. At the first wall the fluid changes into the next BU, leaves that BU through a gap in the back plate into the draining part of the manifold (green).

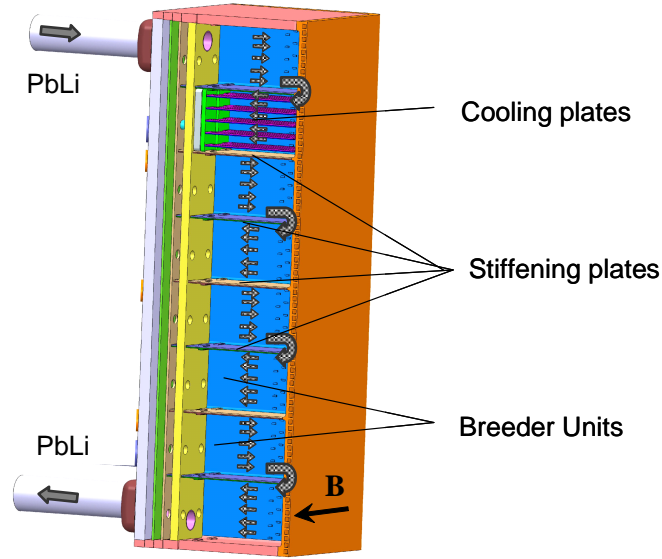


Figure 4: View on a HCLL TBM design proposed by CEA.

number of units is connected to a single supplying line. Here we face the problem of high MHD interaction, associated with high pressure drop. Moreover, breeder units are subdivided by cooling plates into a number of sub-channels. Uniform partitioning between sub-channels and between individual breeder units is another issue that has to be ensured during blanket performance.

Theoretical and experimental MHD analyses focused in the past on forced flows in individual ducts, separated perfectly from each other (see e.g. Bühler (1995)). We are currently in a position that such flows including those which are driven by thermal buoyancy (Bühler (1998), Kharicha, Molokov, Aleksandrova and Bühler (2004), Bühler and Wetzel (2006)) can be predicted in a sufficiently accurate way for fusion relevant parameters in many different geometries. An analysis for an HCLL blanket module based on a decomposition of the geometry into basic elements shows that the major part of pressure drop is expected to occur in circular feeding and draining pipes and in poloidal manifolds (Bühler (2005)). When the flow passes through the gaps in the back plate from the manifold into the BUs or from the BUs into the manifold further contributions to pressure drop have been predicted. The pressure drop along the radial direction in the BUs, however seems negligible in comparison to the previously mentioned ones.

Nevertheless, the HCLL blanket involves several phenomena which are yet not predictable by numerical or analytical analyses and require therefore experimental investigations. Such phenomena are related to the fact that the cooling plates are electrically conducting and provide electrical coupling between neighboring channels. This may have a positive influence if currents arrange in such a way that they homogenize flows in individual fluid regions. On the other hand, electrical coupling could also drive the flow along unexpected paths leading to closed recirculation loops, higher pressure drop, etc. With respect to the tritium content in the blanket, closed recirculation loops are as critical as stagnant regions, since there exist no efficient convective exchange of a dissolved species towards the purification system. A numerical study that consid-

ers the complete electric flow coupling in the blanket for assumed fully developed conditions in a middle cross section of the module, demonstrates the strong interaction of sub-channels in a BU, whereas only a weak coupling is found between neighboring BUs (Mistrangelo and Bühler (2008)).

To confirm first theoretical predictions an experimental campaign has been prepared in which the MHD flow in a prototypical mock-up of a HCLL blanket is investigated in the liquid metal MHD laboratory MEKKA of the Forschungszentrum Karlsruhe. While a full 3D numerical solution of the problem is presently not available for very strong magnetic fields, the experimental data define the scaling laws which are required for the development of a reliable test blanket for ITER.

Another unknown effect may arise from the non-uniform electric conductance of the cooling plates, due to their internal structure with helium channels. The cooling channels result in non-isotropic conductance of the walls with yet unpredictable implications on the flow. This point will require further theoretical and experimental investigations which are out of the scope of the present work.

2 Flow conditions in a HCLL blanket

The inductionless magnetohydrodynamic flow of electrically conducting fluids like liquid lead lithium in a HCLL blanket module is governed by the balance of momentum, Ohm's law, and conservation of mass and charge:

$$\frac{1}{N} \left[\frac{\partial \mathbf{v}}{\partial t} + (\mathbf{v} \cdot \nabla) \mathbf{v} \right] = -\nabla p + \frac{1}{Ha^2} \nabla^2 \mathbf{v} + \mathbf{j} \times \mathbf{B}, \quad (1)$$

$$\mathbf{j} = -\nabla \phi + \mathbf{v} \times \mathbf{B}, \quad (2)$$

$$\nabla \cdot \mathbf{v} = 0, \quad \nabla \cdot \mathbf{j} = 0. \quad (3)$$

In these equations the vectors \mathbf{v} , \mathbf{B} , and \mathbf{j} stand for velocity, magnetic flux density and current density, scaled by the reference values v_0 , B_0 , and $\sigma v_0 B_0$, respectively. The pressure scaled by $\sigma v_0 L B_0^2$ is denoted as p and the electric potential normalized with $v_0 L B$ is written as ϕ . A typical length scale of the problem is L and the fluid properties like the density ρ , the electric conductivity σ and the kinematic viscosity ν are assumed to be constant in the considered temperature range.

The flow is governed by two nondimensional parameters, the interaction parameter

$$N = \frac{\sigma L B_0^2}{\rho v_0} \quad (4)$$

and the Hartmann number

$$Ha = L B_0 \sqrt{\frac{\sigma}{\rho \nu}}. \quad (5)$$

The interaction parameter gives the ratio of electromagnetic forces to inertia forces, while the square of the Hartmann number stands for the ratio of electromagnetic forces to viscous forces.

For the present design of a HCLL blanket a typical length scale is the toroidal dimension of a breeder unit. In order to stay within common MHD notation we introduce the characteristic length L as the half of the BU's toroidal extension, i.e. $L = 0.09$ m and we use the average velocity in a BU to define the velocity scale $v_0 = 1$ mm/s. With the material data for PbLi near 550°C according to Jauch, Karcher, Schulz and Haase (1986) we find for a magnetic field of $B_0 = 5$ T the values

$$Ha = 1.1 \cdot 10^4, \quad N = 1.8 \cdot 10^5. \quad (6)$$

For applications in fusion HCLL blankets both parameters Ha and N reach very high values so that inertia and viscous forces are of minor importance in most of the flow domain. Viscous forces are present only in thin boundary layers or in internal parallel layers. The flow is dominated by a balance between pressure forces and Lorentz forces in the cores of the fluid domains.

Electric currents close their circuits through the electrically conducting walls. The electric resistance of the walls limits the current density in the cores and gives thereby an upper limit for pressure drop. Neighboring channels may communicate through electrically conducting common walls by exchanging electric currents across those walls. This leads to a so-called flow coupling.

The wall conductivity in tangential direction is usually expressed through the wall conductance ratio

$$c = \frac{\sigma_{w,e} t_w}{\sigma L}, \quad (7)$$

where $\sigma_{w,e}$ stands for the effective electric conductivity of the wall with thickness t_w . In the actual design the wall thickness varies between 15 mm for the back plates and 6.5 mm for cooling plates. The effective conductivity takes into account that most of the walls have a “porous” structure, i.e. those walls are perforated by internal helium cooling channels. As a result the effective electric conductivity of these walls is reduced sometimes by a factor of 2 or more depending on the “porosity” ε that denotes the volume fraction of helium in a wall with conductivity σ_w

$$\sigma_{w,e} = (1 - \varepsilon) \sigma_w. \quad (8)$$

At common walls between two adjacent flow domains we must take into account that one wall carries the tangential current of two flow sub regions. The effective wall thickness with respect to one fluid domain is therefore only half the value than that shown in (7). This leads to values for the wall conductance ratios on the order of $c = 0.04$ for the stiffening plates and $c = 0.2$ for the back plate. For most of the walls we find that c is a small quantity, i.e. $c \ll 1$.

For the conductance through the walls one has to consider the wall-normal conductance parameter

$$s = \frac{\sigma_{w,e} L}{\sigma t_w}. \quad (9)$$

This nondimensional group characterizes the conductivity of a wall in its perpendicular direction and it gives an indication for the ratio of potential difference across a fluid domain to the potential drop across a wall. For large values of s , i.e. for thin walls, the variation of potential across the wall is negligible. Applied to HCLL conditions, s is as large as 10 or higher. So practically s is a large quantity. This has the consequence that currents may pass through common walls almost without electric resistance. As a result, the electric potentials on both sides of the wall become approximately equal, which leads to a strong electric flow coupling between neighboring domains.

The pressure drop depends in general on all these parameters. As an example we may consider plane Hartmann flow, where the nondimensional pressure gradient evaluates according to Müller and Bühler (2001) as

$$\nabla p = \frac{1}{\hat{u} (1 - Ha^{-1} \tanh Ha)}, \quad \text{with} \quad \hat{u} = \frac{c + 1}{c + Ha^{-1} \tanh Ha} \quad (10)$$

For $Ha \gg 1$ these expressions simplify to

$$\nabla p = \frac{c + Ha^{-1}}{c + 1} \quad (11)$$

and for MHD flows in electrically conducting ducts under fusion relevant conditions, where usually $Ha^{-1} \ll c$, the latter equation simplifies further to

$$\nabla p \approx \frac{c}{1 + c}. \quad (12)$$

The nondimensional pressure drop then evaluates as

$$\Delta p \approx \frac{c}{1 + c} \Delta l, \quad (13)$$

where Δl denotes the scaled length of the channel, i.e. a nondimensional coefficient accounting for the total geometry under consideration. A similar scaling is expected also in 3D applications

at least at low speed, in the inertialess limit when $N \rightarrow \infty$. The total pressure drop over the whole test section is then expressed as

$$\Delta p = \frac{c}{1+c} A \quad (14)$$

and A describes the influence of the geometry on the flow. For higher velocity, A depends in addition on the Reynolds number, $A = A(Re)$. A dependence of A on the strength of the Hartmann number is expected only for values of Ha lower than those in fusion applications. It is one of the major purposes of the present experiments to investigate the dependence of A on both parameters, Ha and Re (or N) to define an engineering correlation for pressure drop as

$$\Delta p = \frac{c}{1+c} A(Ha, Re; N). \quad (15)$$

This correlation ensures the transferability of the derived scaling laws from the experiments, where NaK is used as a model fluid in a test section fabricated from stainless steel, to TBM conditions, where the fluid is PbLi contained in a structure fabricated from Eurofer. The different material properties of walls and fluids enter the nondimensional correlation only through the wall conductance parameter c , while the parameters that control the flow behavior are taken into account in the function A .

A correlation of the type proposed in (15) has been tested by asymptotic simulations of flows in some basic elements of a TBM for different wall conductance ratios c . It could be observed that the pressure drop scales almost linearly with $c/(1+c)$ in the relevant range of parameters and linearly with c , if c is small. Small deviations from the linear dependence are caused mainly by 3D effects for which the additional pressure drop increases in a slightly weaker form. Nevertheless it was found that the assumption of a linear dependence is conservative when we extrapolate the mock-up results to TBM conditions.

3 Test section

3.1 Design of the MHD mock-up of an ITER TBM

The magnetohydrodynamic parameters for a HCLL blanket and the pressure drop correlations have been outlined in the previous section. In order to investigate the MHD flow in a geometry relevant to the HCLL TBM, in particular for determining a pressure drop correlation, a scaled mock-up of the blanket module has been designed and fabricated at the Forschungszentrum Karlsruhe. A major constraint is the experimental space available in magnet used in the laboratory. The test section has to fit into the large normal conducting magnet of MEKKA laboratory. The total volume of the magnetic gap is quite large and measures about $2000 \times 483 \times 168 \text{ mm}^3$, where the magnetic field lines are aligned with the short dimension. The region in which the magnetic field is sufficiently uniform has the size $800 \times 483 \times 168 \text{ mm}^3$. For reliable results the experiment should fit within this domain. Experience from previous experiments shows that below and above the test section one needs at least 10 mm and 40 mm, respectively, for insulation and instrumentation. Therefore the maximum extension of the test section along magnetic field lines (the toroidal direction in the HCLL module) is roughly 100 mm. This suggests a scale of 1:2 for a breeder unit. For completing the flow path we need at least two BUs and in order to study the MHD effects in poloidal manifolds at least 4 units are required. In principle it would be possible to insert a column of 6 BUs in the MEKKA magnet. However, in order to keep the manufacturing costs acceptable a number of 4 BUs has been chosen. A flow scheme of the mock-up is shown in Fig. 5.

Once the maximum major dimensions are known it is straightforward to scale every geometric element in the HCLL mock-up, based on the TBM reference concept as described by Rampal et al. (2005). This has been done for the stiffening plates, the cooling plates and for the back plate. Walls which have internal helium channels in the HCLL TBM are designed in the experiment as solid walls. The thickness of these walls is reduced further according to their “porosity” or their steel content, in order to achieve comparable electric conductance as in the original design. Exterior walls which separate one column of BUs from another one are considered only with half of their thickness. The other half in a TBM will contribute to the neighboring column. Solid wall in the HCLL such as those of the circular access tubes, for the poloidal manifold or for the back plate are taken directly with their scaled thickness. A view on the MHD mock-up design is shown in the Figs. 6 and 7. Detailed design drawings can be found in the appendix.

3.2 Fabrication

For various reasons described in the earlier reports it was decided to manufacture the central part of the mock-up from a solid piece of material by spark erosion technique. The thin walls, which remain at the end of this process, make it necessary that the raw material has high quality. This is realized by using a forging part to avoid danger of lamination. The back plate with the poloidal manifold and the first wall are also made from the same material. Corners between horizontal and vertical stiffening plates are realized with a scaled radius of 3 mm. The connections between stiffening plates and cooling plates are fabricated as sharp as possible, i.e. with a radius of 0.43 mm. All parts have been checked for correct dimensions, oxides on all surfaces have been removed by chemical cleaning, and the test section was welded using tungsten

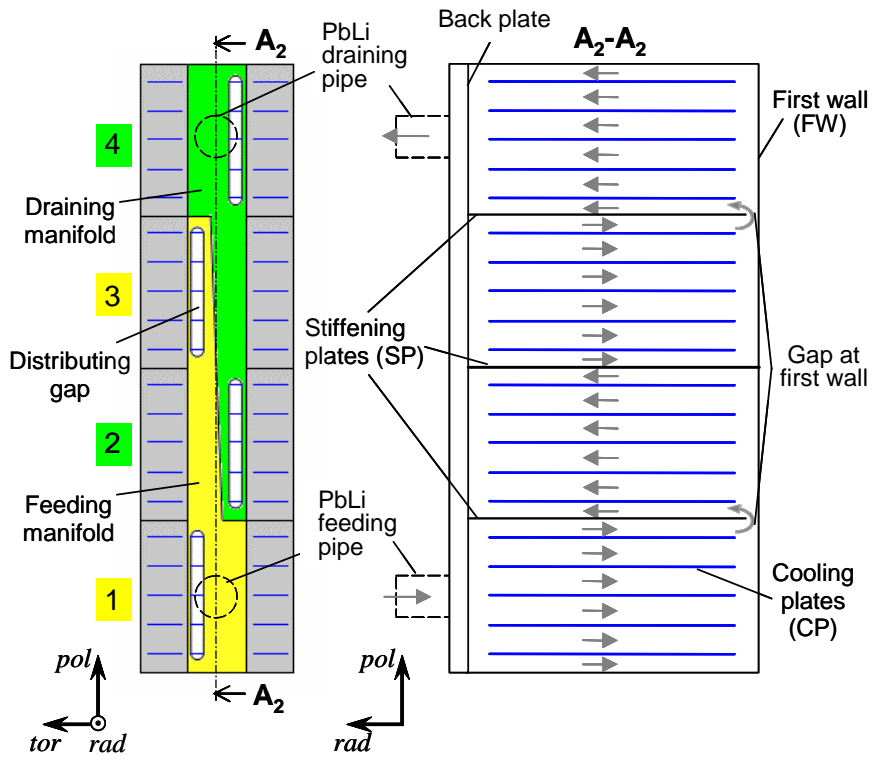


Figure 5: Schematic representation of the flow paths in the MHD mock-up of the TBM.

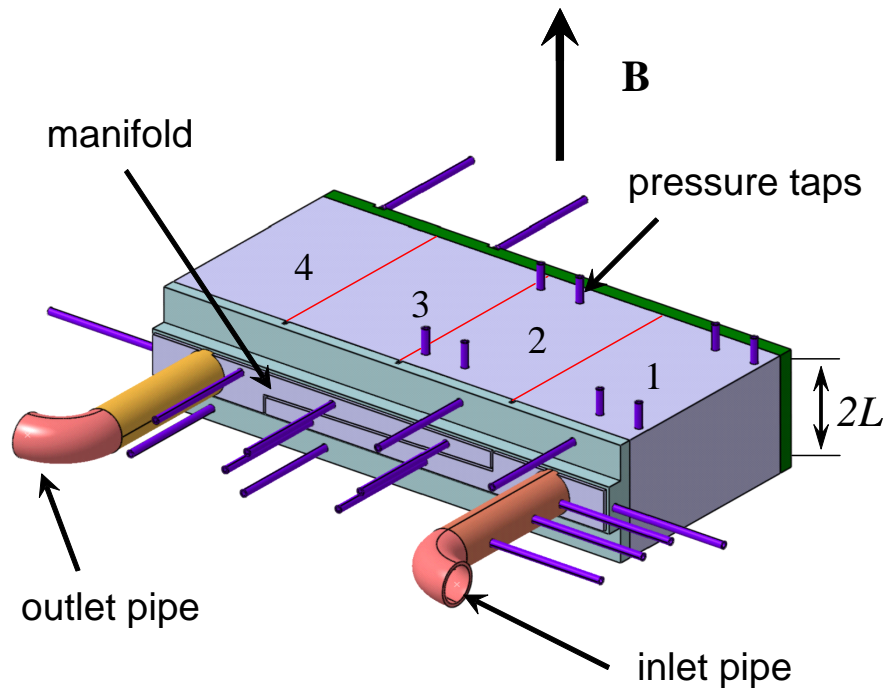


Figure 6: Test section consisting of 4 breeder units, manifolds, inlet and outlet pipes. Pressure differences are measured at 27 pressure taps.

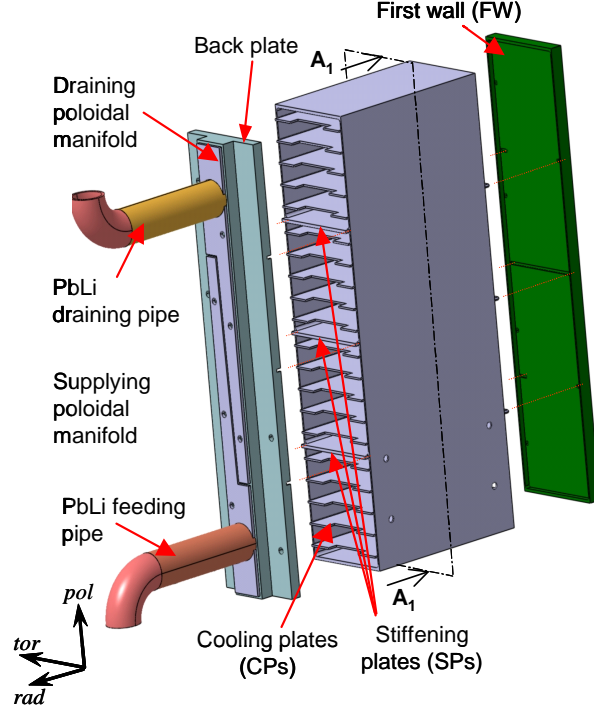


Figure 7: View on the opened MHD mock-up of the TBM showing internal structures.

inert gas technique and electron beam welding. Figure 8 shows the central piece of the mock-up after spark erosion. Then all parts of the test section were assembled. Gas-shielded tungsten-arc welding is a qualified welding process for high-alloyed steel, of which the TBM consist. A further advantage of this process is the high quality of welding seams with a quite smooth surface. The latter point seems important to reduce disturbances of the flow. An intermediate step during welding is shown in Fig. 9.

After the welding was finished a pressure test was performed. This is required before inserting the test section into the liquid metal loop, in order to be able to operate the experiment at pressure levels up to 6 bar and to guarantee safe operation with the chemically reactive fluid NaK. All connections for pressure measurements have been closed and an argon test pressure has been applied. The pressure tests were done in two steps. The first one was a test for leak detection which was performed at a lower pressure level up to 1.5 bar. By using a leak detection spray on the surface of the test section and especially at all welds it was ensured that the seams were perfectly tight. The second one was the main pressure test. Usually pressure tests are performed by using pressurized liquids (preferentially water) as test fluids. The use of water inside the module is not advised here since the experiment will be operated later with the alkali alloy NaK that reacts heavily even with small amounts of water that might be trapped in internal gaps in the test section. Water could also result in the formation of additional oxides on the walls which have to be removed later during the high-temperature wetting procedure. For these reasons the pressure test was done using argon as inert gas. The accomplishment of the pressure test is based on the "AD2000 – Merkblatt" HP30. According to this document

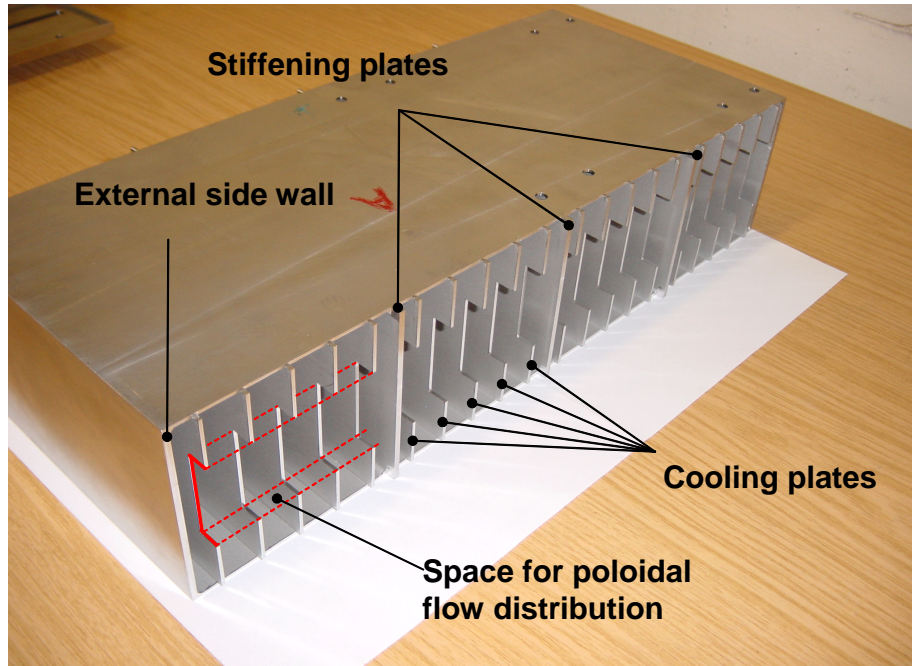


Figure 8: Central part of the MHD mock-up with stiffening and cooling plates. The space for poloidal flow distribution is clearly visible.



Figure 9: Module during welding. The vertical wall in the foreground of the picture is already welded, the upper walls are fixed.



Figure 10: MHD mock-up submersed in water for leak and pressure tests.

the test has to be performed with an internal pressure that exceeds the operational pressure by a factor of 1.3 if the test is done with water and by a factor of 1.1 if the test is done with gas. The test section has been tested successfully up to an internal gas pressure of 6.2 bar, which permits now pressure levels during operation up to 5.6 bar. During the pressure test the module has been put into an "aquarium" (see Fig. 10) for detection of eventually occurring leaks or cracks. In order to guarantee the test pressure of 6.2 bar two independent manometers have been used. One manometer was mounted directly on the TBM. The big analogue display allowed safe metering with distance of 10 m. The second manometer was installed directly on the pressure reducer of the compressed gas cylinder. During the pressure test both manometers showed same values. The protocols of the leak and pressure test are shown in the appendix.

3.3 Wetting procedure

After all leak tests have been completed and the tightness of the test section was guaranteed the module has been installed in the liquid metal loop of the MEKKA laboratory. The internal surface of the module is usually covered by a layer of oxides or other impurities that react with the wall material during the production process of the individual parts or during welding. Those layers may create a contact resistance between the liquid metal and the wall and may therefore change the magnetohydrodynamic performance in comparison with the ideal case when no contact resistance is present (see e.g. Bühler and Molokov (1994)). For that reason a high-temperature wetting procedure is performed with the installed mock up with the purpose of dissolving the wall-attached impurities or oxide layers into the liquid metal. The test section has been especially prepared for this procedure by adding a thick thermal insulation. The liquid metal heating is provided by the loop and by additional heaters at the supplying piping system.

The installed test section is shown in Fig. 11 and fitted with thermal insulation in Fig. 12.

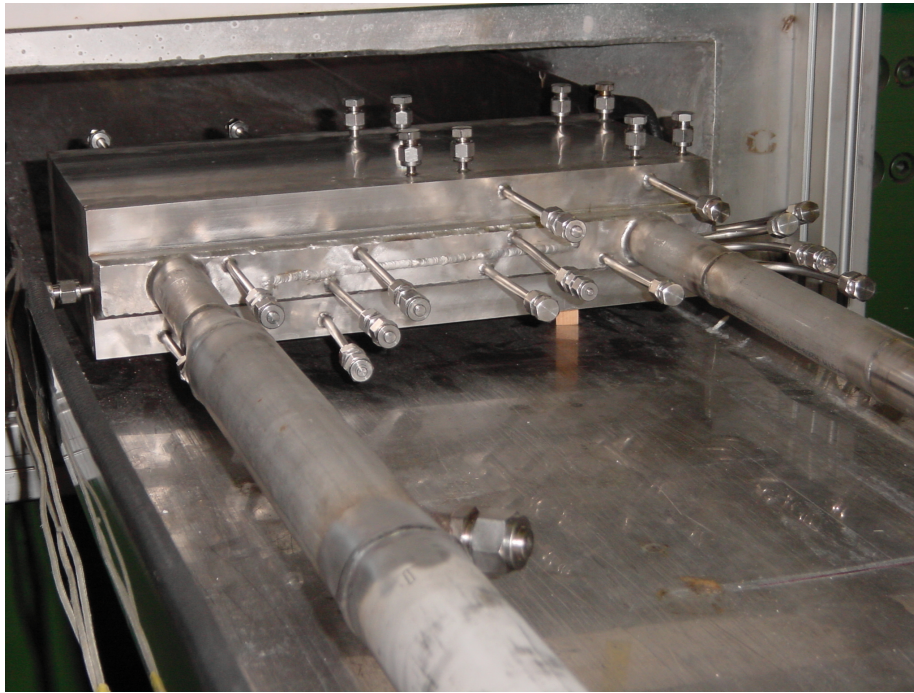


Figure 11: Module installed in the liquid metal loop. The pressure taps are still closed by caps in this stage of installation.

For wetting and removal of oxides the test section is maintained at temperatures close to 300 °C. A cold trap is operated in a bypass that forms the purification loop of the liquid metal circuit. For details see Fig. 15. The dissolved impurities precipitate in the cold trap on the large surface of a dense wire mesh at lower temperatures around 30 – 40 °C. A typical temperature record of a daily wetting cycle is displayed in Fig. 13. This procedure was repeated for 15 days

After finishing the wetting procedure the insulation was removed and the installation of pressure measuring lines and surface potential electrodes has been completed.

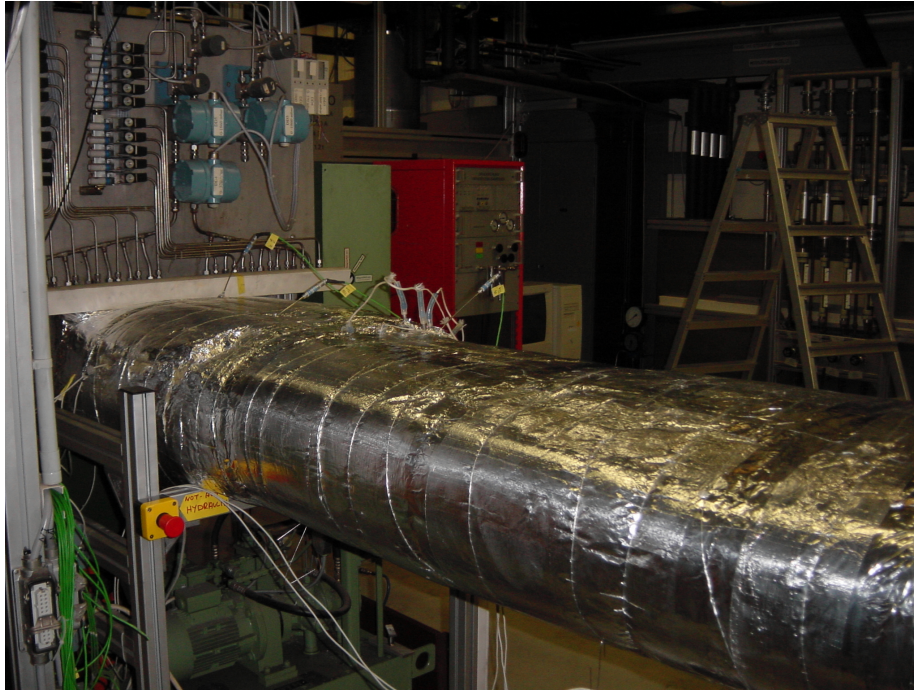


Figure 12: Module with thermal insulation.

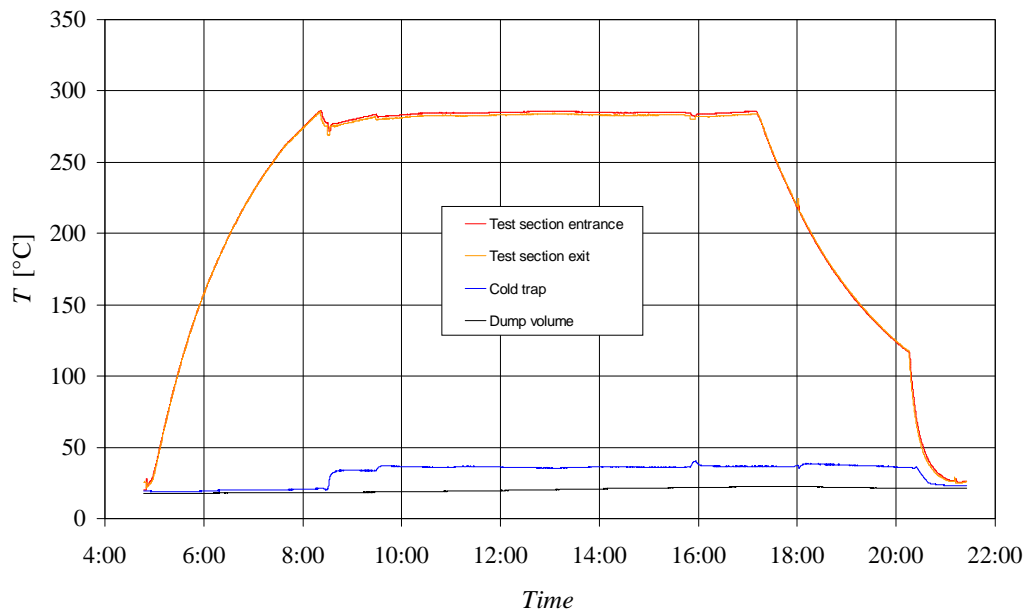


Figure 13: Typical temperature record of a daily wetting cycle. The test section is kept close to 300 °C, the cold trap near 40 °C.

4 The MEKKA laboratory

The MHD mock-up experiments are performed in the MEKKA laboratory of the Forschungszentrum Karlsruhe. The measuring techniques used in the MEKKA-facility have been described previously in a detailed report by Barleon, Mack and Stieglitz (1996). In the following we summarize and restrict the description to the elements most relevant for the present investigations. The photograph of MEKKA-facility, in which the MHD mock-up has been inserted, is shown in Fig. 14.

4.1 Liquid metal loop

An eutectic sodium-potassium alloy (Na22K78) is used as model fluid in the liquid metal loop. Its thermophysical properties according to Foust (1972) are:

T [°C]	ρ [kg/m ³]	ν [10 ⁻⁶ m ² /s]	σ [10 ⁶ 1/Ωm]
20	868.4	1.05	2.88
40	863.2	0.902	2.79
60	858.1	0.834	2.70

NaK has a lower density and a higher electrical conductivity compared to a eutectic lead lithium alloy PbLi foreseen in the blanket design. This allows in the present experiments to reach, with the available magnet (2 T), high Hartmann numbers up to $Ha = 5800$ which are not too far from fusion applications.

Figure 15 shows a sketch of the liquid metal loop. A canned motor pump with a maximum pressure head of 0.9 MPa at a flow rate of 25 m³/h circulates the liquid metal at temperatures below 250 °C. An additional electromagnetic pump is used for very low flow rates and for high temperature runs e.g. during the wetting procedure. Due to the technical features of the loop and the magnet, the MEKKA facility is capable of attaining interaction parameters in the range of $N = 10^2 - 10^5$, which are appropriate for applications in liquid-metal fusion blankets.

The whole liquid metal loop with pumps, dump volume, expansion tank, heat exchanger, cold trap, pressure transducers, controlling valves etc. is mounted in a rack, which is movable on rails by means of a hydraulic piston with a stroke of 2500 mm. The arrangement of a movable loop with connected test section enables the operator to place the test section at any desired position relative to the fixed magnet. This allows a good manual access to the instrumented locations of the test section and variable positioning of the experiment within the magnet. Thus, special measurement positions of the test section within the magnetic field can be realized.

The dump volume is fabricated of stainless steel and has a volume of 0.28 m³. It is filled with 0.2 m³ of sodium-potassium (NaK). It is foreseen to contain the whole liquid metal volume in non-operation time. Filling of the loop is achieved by a slight argon over-pressure on the dump volume in order to press the liquid into the loop. After successful filling, pressure equilibration between the top and bottom gas system is established. Draining of the loop after operation and in case of an emergency is performed by gravity.

Accidental liquid metal leaks are detected by short-cut electrodes, which are placed below the rack. In case of a leak these detectors send a signal to a programmable logic controller, which then organizes automatically the shut down of the loop operation and starts the security tasks. In order to ensure a safe operation all systems have to be helium leak tight to avoid alkali-oxide reactions.



Figure 14: View on the liquid-metal NaK loop in the MEKKA laboratory.

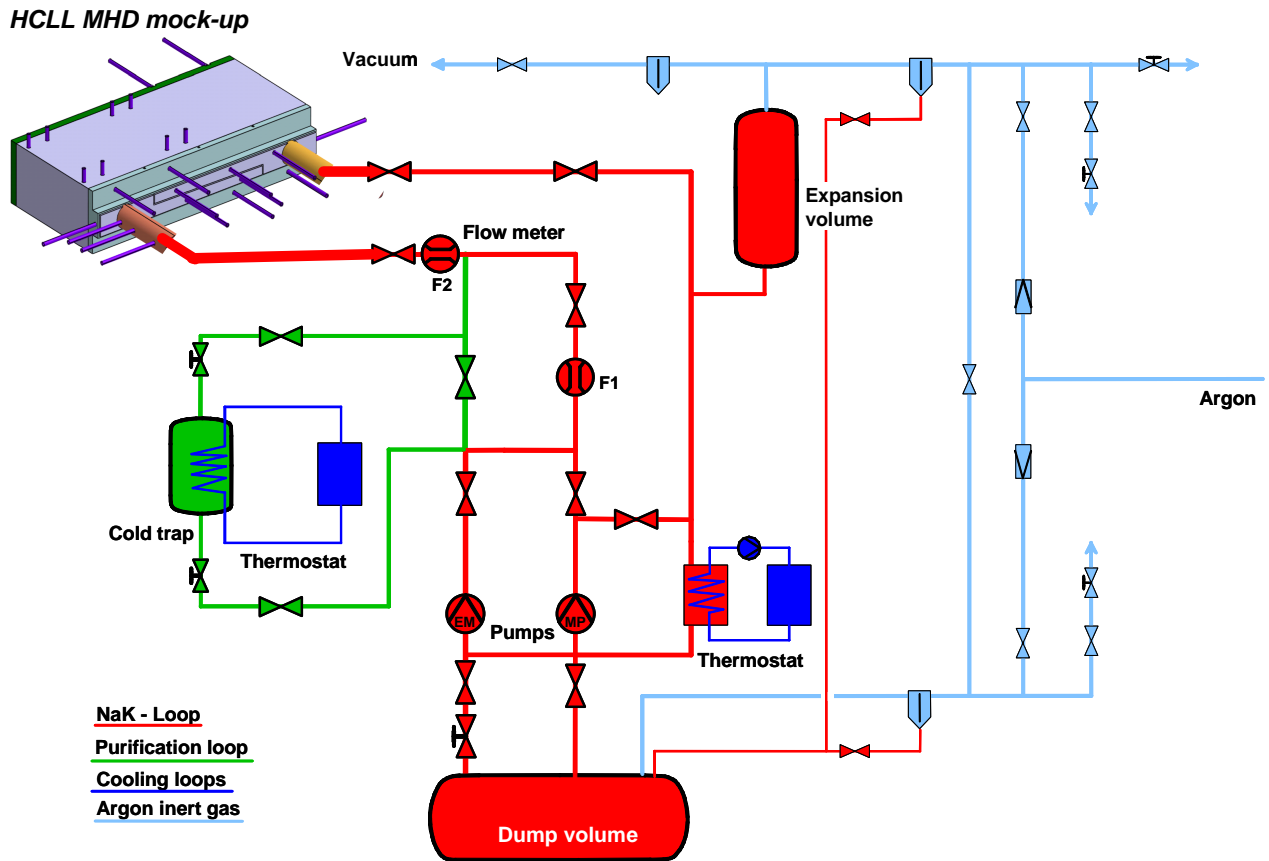


Figure 15: Schematic of the liquid metal NaK loop in the MEKKA laboratory. Colors indicate different parts of the total system. Red: liquid metal loop with HCLL mock-up; green: purification loop; blue: oil cooling loops (water cooling loops are not shown); light blue: argon inert gas system.

The purification loop consists mainly of the cold trap with its thermostat and electromagnetic flow meters. At high temperatures above 300°C during the wetting phase a large part of the oxides is dissolved in the liquid metal. In the cold trap the oxides and other impurities are precipitated on a wire mesh and separated from the liquid. The separation process takes advantage of the weaker solubility of the oxides in pure NaK at lower temperatures. For this purpose the NaK in the cold trap is cooled by an oil filled thermostat.

The loop with all its systems is totally remote controlled from the operation room. Due to the large amount of components, alarm and level detectors a fully manual operation and a visual control is hardly possible. Moreover, in case of an accident quite a lot of steps have to be made almost simultaneously or in a defined time sequence. Therefore, all critical components are connected via alarm sensors to the input gates of a programmable logic controller that prevents the facility from a maloperation by a user. If critical signals are detected the operator receives an optical and acoustic warning and in cases that concern the safety of the system an automatic shut down and draining of the loop is initiated.

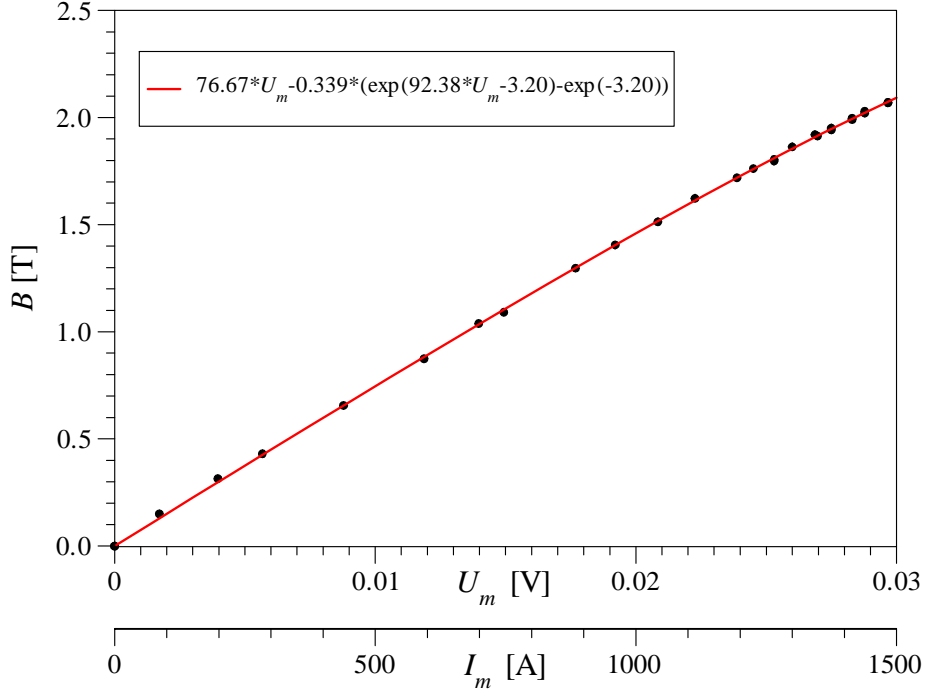


Figure 16: Calibration of magnetic field with measured voltage signal.

4.2 Magnetic field

The uniform transverse magnetic field is provided for this experiment by a normal conducting dipole magnet. Its maximum field strength is 2.1 T. The magnetic field has a vertical orientation. The magnetic gap used for the experiment has cuboidal shape and within a region of $800 \text{ mm} \times 480 \text{ mm} \times 168 \text{ mm}$ the field is quite uniform with deviations from the core value smaller than 1%. The operation of the magnet requires a variable DC power supply with voltage and current up to 300 V and 1500 A. This is provided by a transductor fed by three phases from the general power supply. The magnetic field \mathbf{B} depends approximately linearly on the applied current I_m . However, for higher magnetic fields the magnet feels already weak saturation which is shown by a slightly nonlinear behavior. This nonlinearity is taken into account by a calibration fit of measured field intensities as shown in Fig. 16. A measured shunt voltage U_m in a range $0 \text{ V} < U_m < 0.03 \text{ V}$ corresponds to currents I_m in the range between $0 \text{ A} < I_m < 1500 \text{ A}$.

4.3 Flow rate measurements

An important property for the investigation of MHD flows is the total mass flow rate or the volumetric flow rate (required to define the mean velocity v_0) through the test section. In order to achieve accurate and redundant results two different types of flow meters are used. One is a so-called gyrostatic (Coriolis) mass flow meter and the other is an electromagnetic flow meter. The results obtained by the Coriolis flow meter are independent of the kinematic viscosity and the temperature. The instrument can be adjusted continuously in its measurement range from $\dot{M}_1 = 0 - 3840 \text{ kg/h}$ to $0 - 76000 \text{ kg/h}$ via remote control. It offers the possibility to a self-calibration if the fluid is at rest. The accuracy of the mass flow meter is quite good with

relative errors below 1% of the chosen scale. The operation range of the instrument is limited to temperatures below 200 °C.

The second type of flow meter is an electromagnetic flow meter. The measurement principle is based on Faraday's law, according to which an electrically conducting medium moving through a transverse magnetic field experiences an induced electric field. The latter one can be detected by electrodes welded at the sides of a channel or pipe. The calibration diagram in Fig. 17 shows the almost perfect linearity between volumetric flow rate \dot{M}_1/ρ derived from the Coriolis flow meter and the induced voltage U_2 of this instrument in the considered range of flow rates. Both quantities are related as

$$\frac{\dot{M}_1/\rho}{[\text{m}^3/\text{h}]} = 1.791 \frac{U_2}{[\text{mV}]} - 0.0334. \quad (16)$$

The calibration shows that the Coriolis flow meter has a slight offset that could affect the evaluation of data in the region of small flow rates. For that reason it is more suitable to use the data obtained by the electromagnetic flow meter and to evaluate the volumetric flow rate as

$$\frac{\dot{M}/\rho}{[\text{m}^3/\text{h}]} = 1.791 \frac{U_2}{[\text{mV}]}. \quad (17)$$

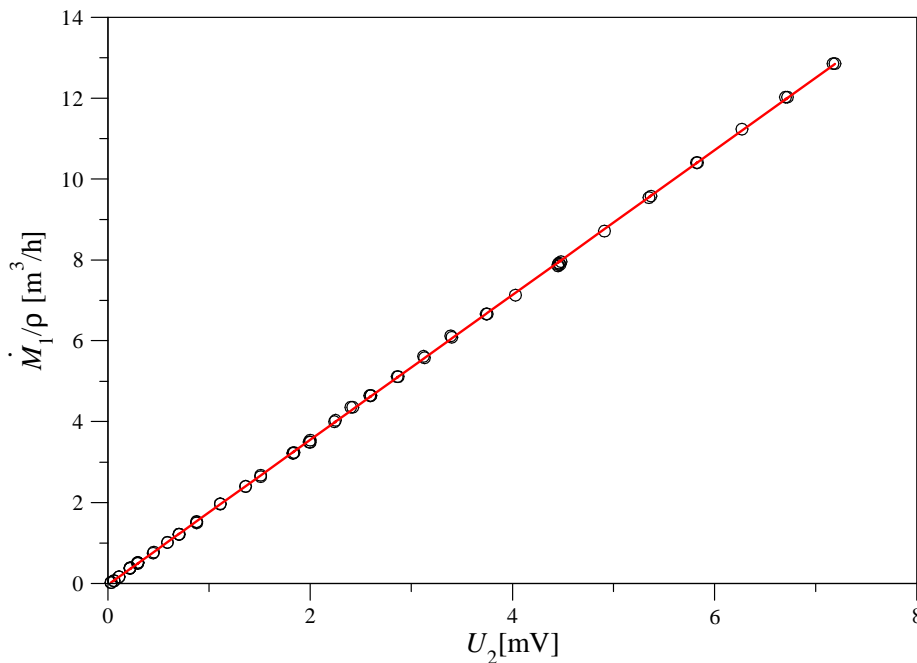


Figure 17: Calibration diagram for electromagnetic flow meter. Volumetric flow rate \dot{M}_1/ρ measured by the Coriolis flow meter F1 versus induced voltage U_2 at the electromagnetic flow meter F2.

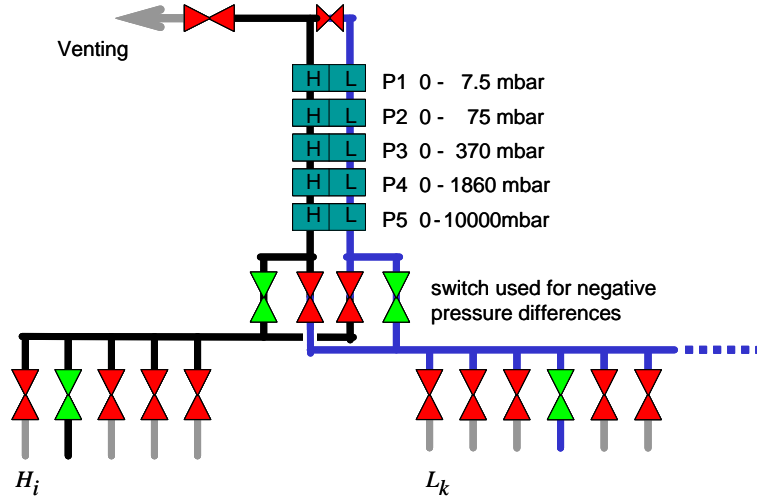


Figure 18: Scheme of the pressure measuring system.

4.4 Pressure difference measurements

The pressure difference measurements are performed in the NaK loop via five capacitive pressure transducers mounted in series. The system is designed to measure a positive pressure difference between one line H_i with higher pressure and another line L_k with lower value, both connected to the test section. In the current installation we have $i = 1, 2, \dots, 5$ and $k = 1, 2, \dots, 24$. The unipolar pressure transducers cannot detect pressure differences of reversed sign. If for some reasons during the experiment the pressure at a line L becomes higher than that at the selected line H it is possible to switch the lines in front of the unipolar transducers. For details see Fig. 18. All transducers are sensing the same pressure difference. In order to avoid measurement errors due to nonlinearities near the end of the measurement ranges individual transducers are overlapping. From all five readings P1-P5 the one with highest accuracy for the measured data range is selected as *the* measured pressure value.

The measurement principle of a capacitive pressure transducer is very simple. A pressure difference deforms membranes and changes their electric capacity. The capacity is transformed to a current (4 mA – 20 mA) that is recorded by the data acquisition system. The errors of the pressure transducers are $\pm 0.5\%$ of the maximum value of the chosen measurement range. An eventual shift of the measurement instrument by temperature changes is compensated by electronics. The operation temperature is limited to 120°C and the maximum pressure allowed at the membrane is restricted to 140 bar.

It is expected that the electric potential may vary strongly over the surface of the TBM model. A connection of pressure taps with the pressure transducers through metallic pipes would lead to some electric short circuit and could modify the flow under consideration. To minimize such undesired effects the pressure lines were connected in a first attempt with non conducting flexible rubber tubing (according to the advice of colleagues who did the same a couple of years ago in another experiment). A photograph of the rubber installation is shown in Fig. 19. It turned out, however, during first experiments that these tubes were incompatible with our liquid metal. After a short experimental campaign most of them were plugged by a dry grey powder-like substance. A first attempt was made for cleaning of these tubes but after

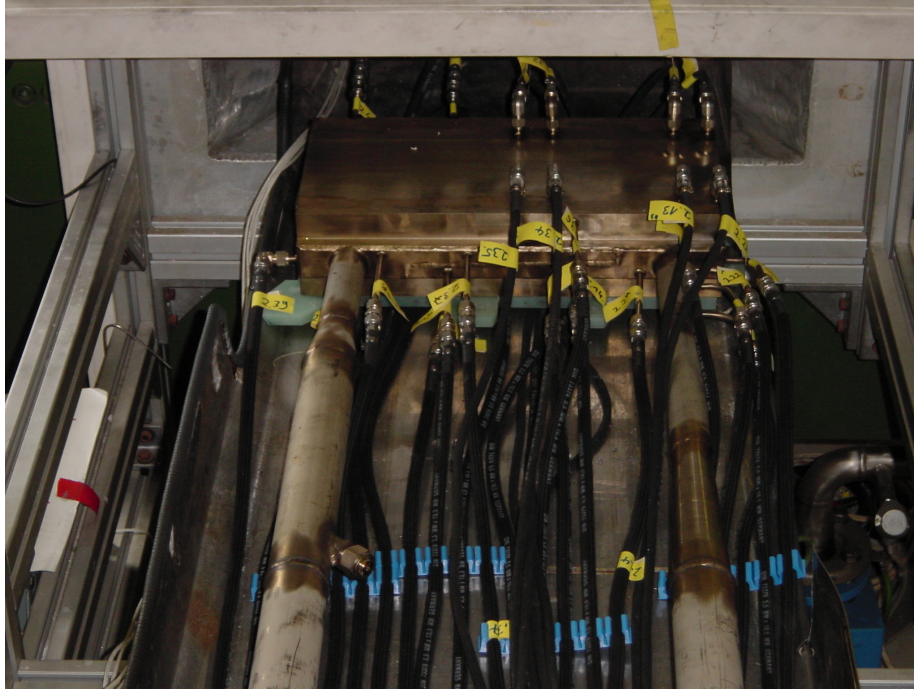


Figure 19: Connection of pressure taps with pressure transducers through flexible rubber tubes.

subsequent plugging the decision was made to install a system based on rigid pipes of stainless steel. This second installation is shown in Fig. 20. The pipes are externally insulated by flexible silicon tubes to avoid that a metallic contact creates a short circuit close to the test section. An electric connection of pipes occurs now only at the pressure transducers after a length of more than 2 m. Therefore the total length for a short circuited current is at least 4 m and considering the small cross section of the pipes (external diameter $d = 6$ mm) their resistance seems high enough to limit the unwanted currents to tolerable values that do not affect the flow in the considered breeder units. This has been confirmed by measurements of the potential drop along the pressure lines from which the leakage currents have been determined and their influence on potential distribution was estimated. It can be shown that the electric perturbations are limited to the immediate vicinity of the pressure taps and that they decay rapidly within a distance much smaller than $2d$.



Figure 20: Connection of pressure taps with pressure transducers through rigid pipes of stainless steel. The pipes are externally insulated by flexible silicon tubes to avoid that a contact with metallic structures creates a short circuit already close to the test section.

4.5 Surface potential measurements

Potential measurements give essential information on the flow structure in the breeder units since the potential can be often interpreted as an approximate streamfunction for the fluid flow and it can be directly compared with theoretical data. According to Ohm's law (2) potential and velocity are coupled as

$$\mathbf{j} = -\nabla\phi + \mathbf{v} \times \mathbf{B}. \quad (18)$$

For many MHD flows at high Hartmann numbers the current density \mathbf{j} is small in comparison with the potential gradient $\nabla\phi$ or the induced electric field $\mathbf{v} \times \mathbf{B}$. For such conditions it is possible to solve the previous equation for velocity components in the plane perpendicular to the magnetic field and we find with $\mathbf{B} = \hat{\mathbf{z}}$

$$u = -\frac{\partial\phi}{\partial y}, \quad v = \frac{\partial\phi}{\partial x}, \quad (19)$$

i.e. we may interpret the electric potential as the hydrodynamic streamfunction. As a consequence of that we can determine the flux of fluid carried between two positions y_1 and y_2 according to

$$q = \int_{y_1}^{y_2} u \, dy = -(\phi_2 - \phi_1) \quad (20)$$

as the difference between the electric potentials ϕ_1 and ϕ_2 measured at these points. This fact is of particular importance since it allows determining the flow rates (mean velocities) in sub-channels formed by the cooling plates and grid plates if potential sensors are placed at the positions where those internal walls are connected with the Hartmann walls. The mean velocity between two potential sensors is then obtained as

$$\bar{u} = -\frac{\phi_2 - \phi_1}{y_2 - y_1}. \quad (21)$$

For this purpose the surface of the test section is covered by insulating plates which carry more than 600 spring-loaded probes for detecting the electric potential. Since the walls are thin, the potential measured on the outer surface of the mock-up equals approximately the potential at the fluid-wall interface.

A principle sketch of two spring-loaded needles used for potential measurements is shown in Fig. 21. The fully instrumented test section with surface potential probes and completed wiring is shown in Fig. 22. The cables are connected with a multiplexer (see Fig. 24) that switches packages of 15 signals to a digital multichannel nano-voltmeter, which resolves electric potential differences up to $\pm 0.1 \mu\text{V}$. The multiplexer and the nano-voltmeter are controlled by a computer.

In order to get more detailed information about potential distribution at positions where 3D effects are expected, i.e. near the entrance to the breeder units at the back plate or near the first wall where the flow is collected and transferred into the neighboring units, a higher spatial resolution has been chosen. The positions of potential probes can be seen from Figs. 25 and 26. The sensors are located in correspondence of the stiffening plates and cooling plates and the potential values recorded at these positions should allow drawing conclusions about flow rates in the individual sub-channels formed by these walls. Similar instrumentations exist also at the first wall, at the back plate and at the ends of the blanket module.

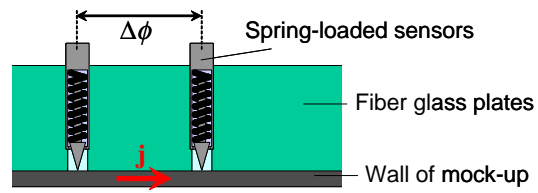


Figure 21: Sketch of spring-loaded potential sensors mounted in insulating fiber glass plates on the outer surface of a current-carrying wall.

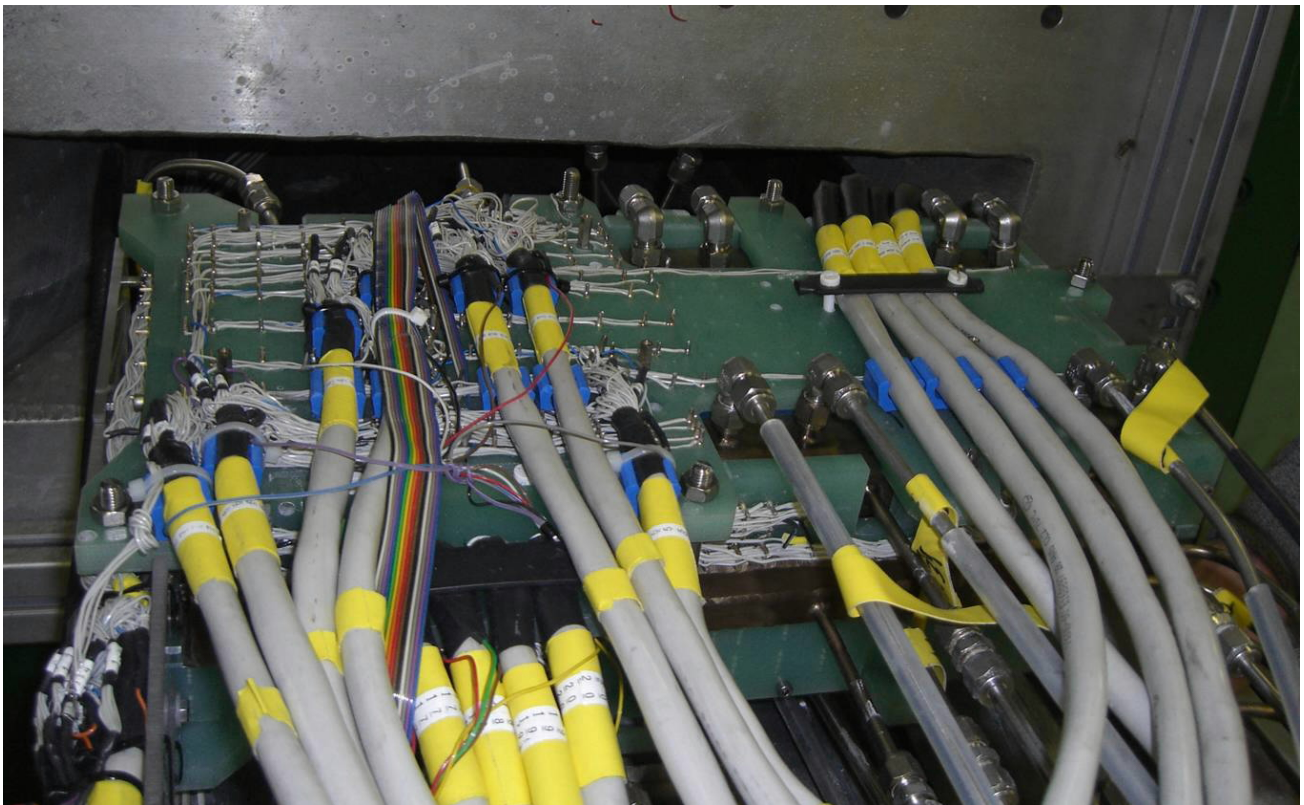


Figure 22: Insulating plates carrying about 600 potential sensors, mounted around the MHD mock-up.

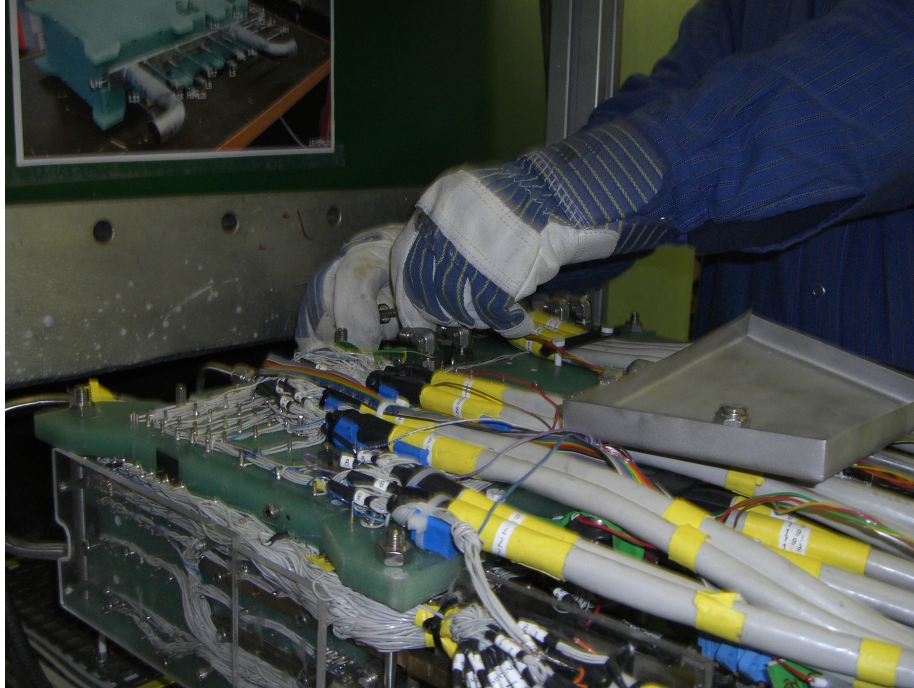


Figure 23: Reconnection of some pressure lines which had been disconnected for installation of insulating plates carrying potential sensors.

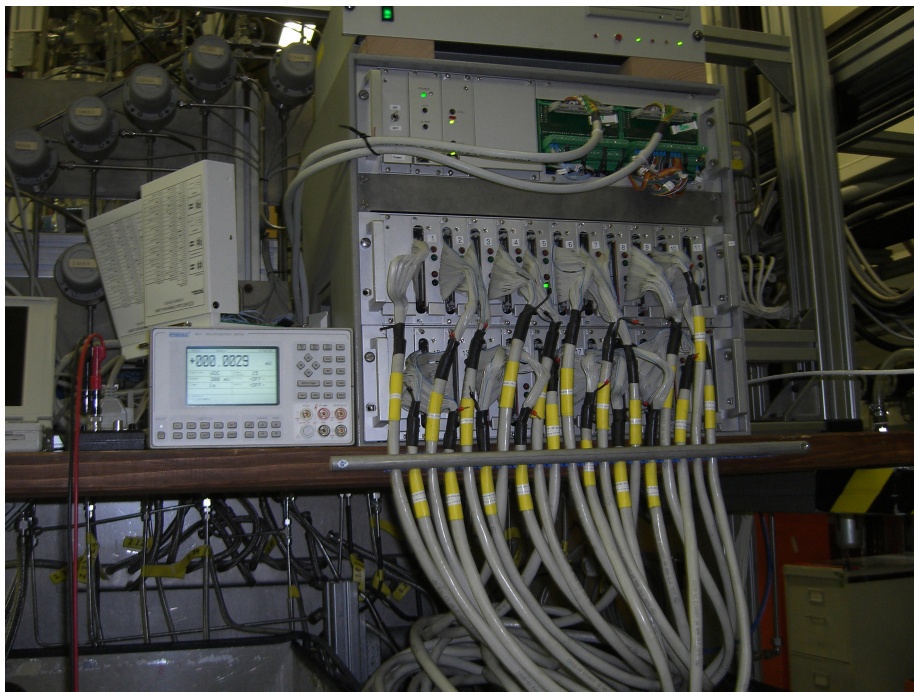


Figure 24: Multiplexer connected to potential sensors.

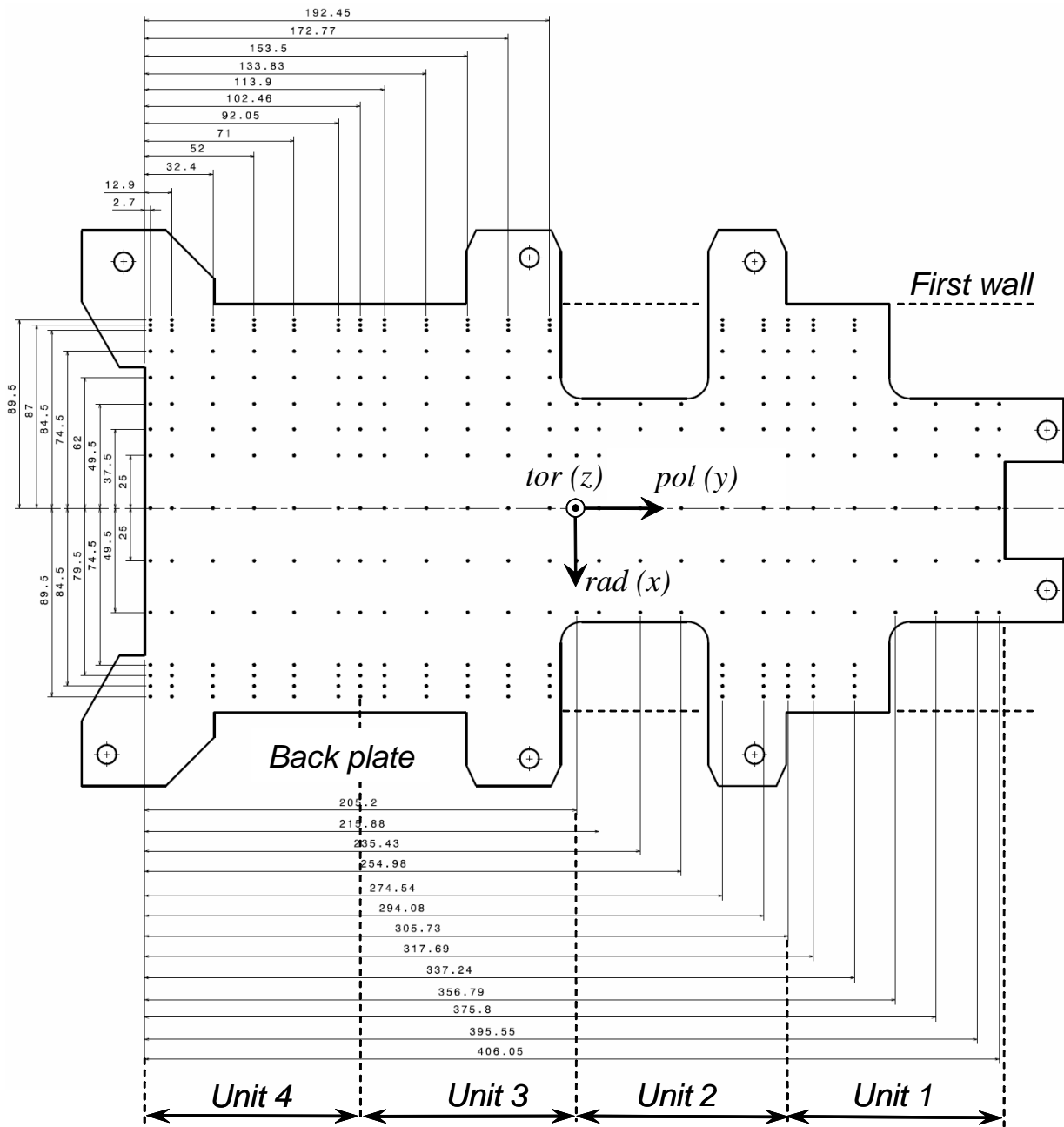


Figure 25: Positions of potential sensors on the upper Hartmann wall measured in [mm].

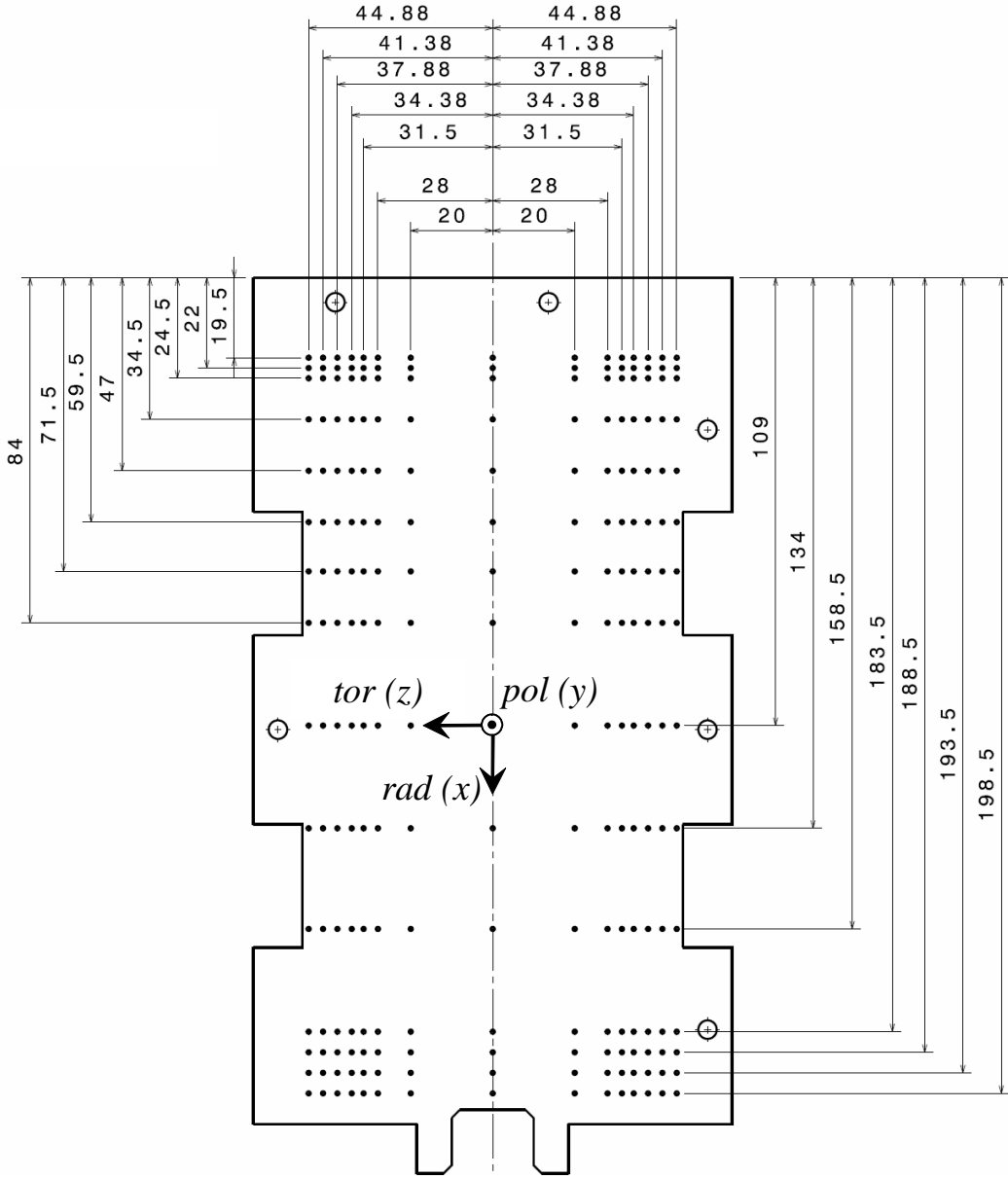


Figure 26: Positions of potential sensors on one external side wall measured in [mm].

4.6 Data acquisition

The measurements were controlled by a computer using a program on the basis of the LabView software. This program controls the valves H_i and L_k of the pressure measuring system, it switches the multiplexer used to measure surface electric potential, it controls and reads the multi-channel nano-voltmeter, the data acquisition cards in the PC etc. Moreover, temperature measurements at the entrance and exit of the test section are used to determine the actual temperature-dependent thermophysical properties of the liquid metal, i.e. $\rho(T)$, $\nu(T)$ and $\sigma(T)$. Together with measurements of B_0 and v_0 it is then possible to determine immediately the governing nondimensional parameters, the Hartmann number Ha , the interaction parameter N or the Reynolds number Re .

The measurements were organized in the following way: the magnetic field and the flow rate are adjusted to give desired Hartmann numbers and interaction parameters. The program then selects automatically one of the 40 levels of the multiplexer. Each level switches 15 potential signals to the multi-channel nano-voltmeter. The potentials are scanned by the voltmeter and send to the PC. For each potential signal an integration time of 1 s is used. In parallel the pressure measurements are performed by automatically scanning through all pressure measuring lines. With this measuring program it is possible to record simultaneously surface potential and pressure variations along the surface of the mock-up.

5 Results

Numerical MHD simulations for the whole 3D geometry at fusion typical parameters are not possible with the present numerical schemes and available computers. For that reason the total geometry of a HCLL blanket was decomposed into major components for which separate analyses have been performed without considering the cooling plates and the electromagnetic flow coupling. One such element is shown in Fig. 27. The global performance is then estimated by combining the single effects in an overall picture as described e.g. by Bühler (2005). As a result it is found that the major part of pressure drop arises from the flow in the circular access tubes, inside the poloidal manifolds and when the flow passes through the distributing and collecting gaps. The pressure drop inside the breeder units instead is small. It is the aim of the present experimental investigations to support previous estimates and to yield results for inertial flows with full electromagnetic coupling for which no simulations are available so far.

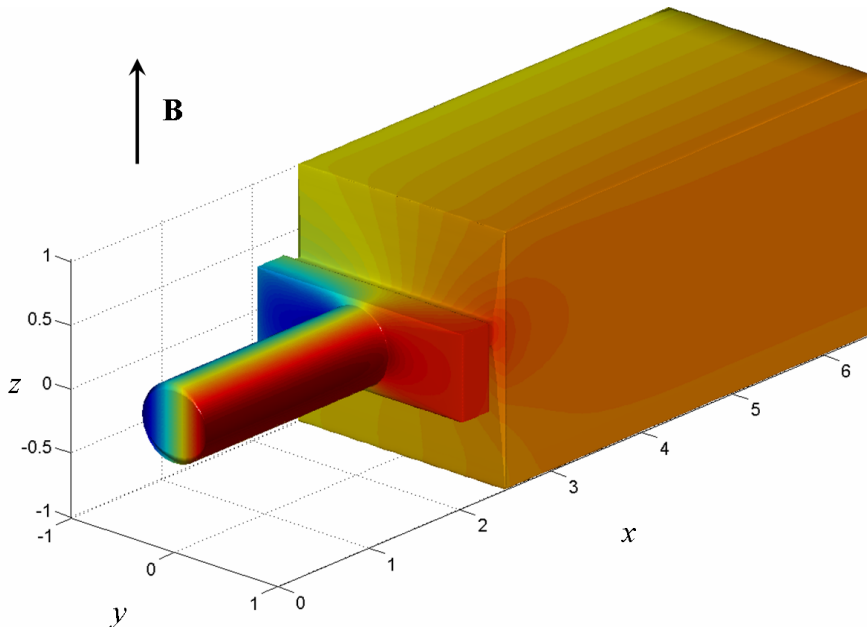


Figure 27: Part of decomposed geometry used for estimates of pressure drop.

Experiments have been performed for a variety of flow rates and values of magnetic field. Flow rates and magnetic fields have been adjusted to desired values and when the flow in the loop reached stationary conditions for all variables (including temperature) the recording of data has been started. Measurements have been performed for the distribution of pressure and electric potential along the surface of the module. Nondimensional results shown in the following sub-sections are presented using magnetohydrodynamic scales for pressure $p_0 = \sigma v_0 L B_0^2$ and for potential $\phi_0 = v_0 L B_0$, respectively, as they were introduced earlier in Sect. 2.

5.1 Pressure measurements

The experiment was supplied with 27 pressure taps for obtaining an overview about the pressure distribution along typical flow paths. The aim is to investigate pressure drops at different

positions to identify locations of larger pressure heads. This point seems quite important for a further development and improvement of this type of blanket. Results of pressure distribution have been combined and plotted in graphs.

Individual flow paths for which experimental results are presented in the following are shown in the sketch in Fig. 28. The flow enters the mock-up through a circular pipe and a poloidal manifold (path AC), it continues flowing in breeder unit 1 along paths DE, then it passes into unit 2 through a gap along the first wall and returns in unit 2 along the lines FG. When the fluid leaves unit 2 it flows along the exit manifold (path HI). Units 3 and 4 are fed and drained in a similar way as units 1 and 2 through the distributing and collecting manifolds.

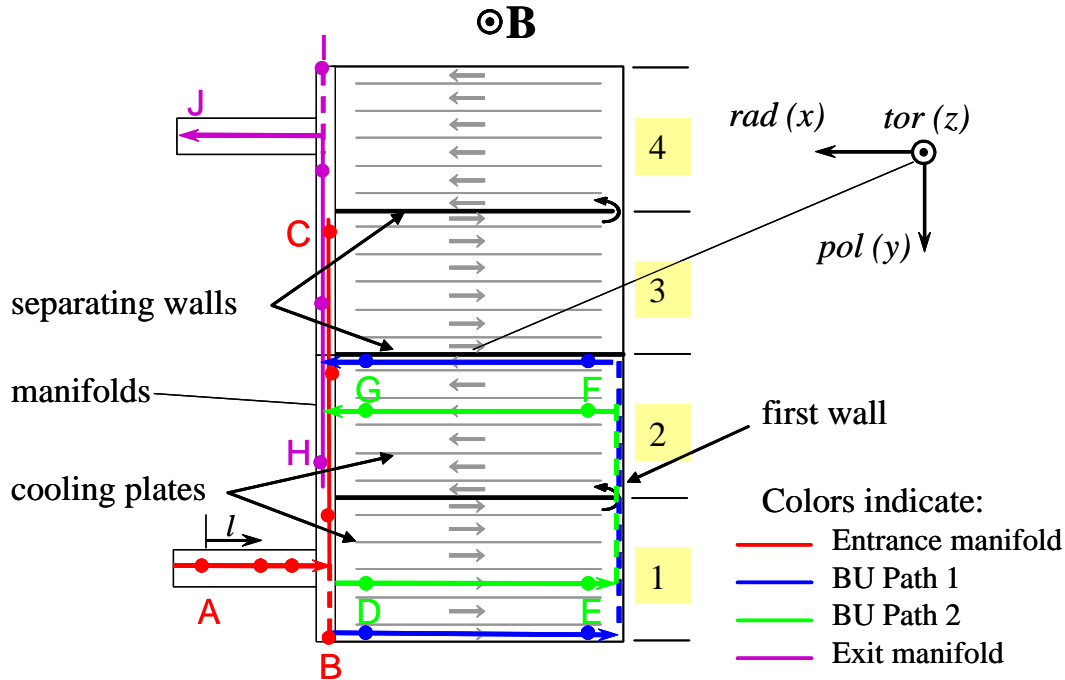


Figure 28: Sketch of the blanket mock-up indicating individual flow paths in circular pipe and entrance manifold (AC), in breeder units (DE and FG) and in exit manifold (HI).

Fig. 29 shows the measured distribution of pressure along the different flow paths in the blanket module, measured with respect to the first pressure tap located at position A. It represents a typical result for high Hartmann numbers. Results are plotted along the “length” l of the flow paths as indicated in Fig. 28 (starting from position A; dash lines excluded). The unique representation of measurements performed at a Hartmann number of $Ha = 3000$ for four different Reynolds numbers $Re = 666 \div 3360$ supports the pressure scaling introduced above. Moreover, it confirms the fact that the MHD flows at fusion relevant conditions, i.e. at high Hartmann numbers and Reynolds numbers as foreseen in the blanket do not depend on inertia effects. The measurements confirm the theoretical predictions that the major part of pressure drop occurs in the circular entrance pipe (AB) and in the manifolds (BC and HI), since the velocities here are much higher than in the breeder units due to the smaller cross sections. Further, the walls of pipes and manifolds are thicker which corresponds to increased electric conductance of the walls compared to the breeder units. This leads to higher currents

and stronger Lorentz forces which create higher pressure drop. Additional contributions to pressure drop occur when the fluid passes through narrow gaps into and out of the breeder units (BD, GH), because at these positions the fluid undergoes strong expansions and contractions. Flows of this kind are known to exhibit strong 3D MHD effects and cause higher pressure drop (Bühler (2008)). The contraction of the flow into a narrow gap between units 1 and 2 (EF) and turning by 180° at the first wall creates no substantial contribution to pressure drop since expansions, contractions and bend flows in a plane perpendicular to the magnetic field do not cause large additional MHD head losses (Molokov (1995)). Compared with the contributions in the manifolds and gaps, the pressure drop of the slow flow in the breeder units (DE, FG) is negligible.

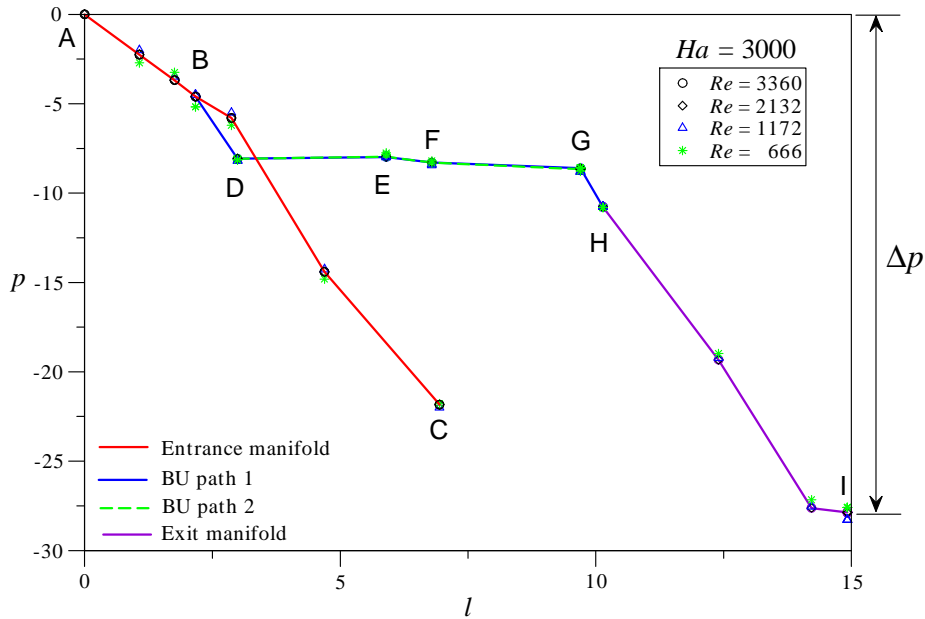


Figure 29: Pressure distribution along typical flow paths of the blanket module for $Ha = 3000$ and different Reynolds numbers.

For higher values of Ha the discussed behavior remains valid and changes compared with these results are only marginal as can be seen for $Ha = 4000$ and $Ha = 5000$ at least for the Reynolds numbers shown in Figs. 29-31. If instead the magnetic field is weaker, inertia effects play a more important role and modify the pressure distribution. This can be seen in Fig. 32, where results for $Ha = 1000$ are displayed. We observe that inertia creates now increasing contributions to pressure drop across the gap along the first wall (EF) with increasing Reynolds number. Further inertial effects can be observed between positions B and D, where the fluid undergoes contractions and expansions into much larger domains. As a result, the velocity drops at B which leads to a pressure recovery according to Bernoulli's equation. When the flow passes through the narrow gap in the back plate into the breeder unit 1 the pressure drops strongly, but downstream of the pressure tap D part of that pressure drop is recovered. Most important is the fact that the total pressure drop now depends clearly on inertia and, as a function of the Reynolds number, it may take values that are much larger than those expected for inertialess flows.

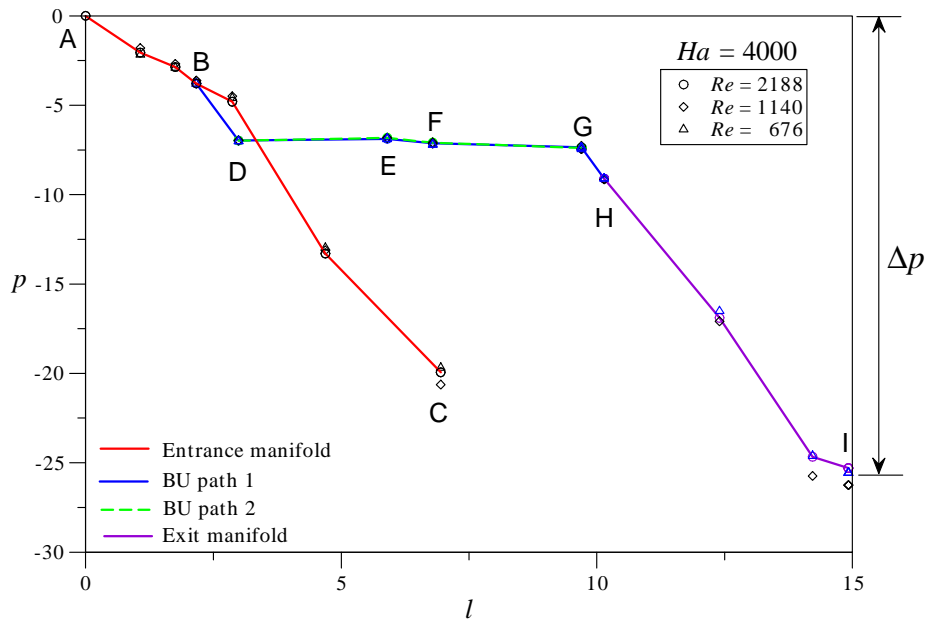


Figure 30: Pressure distribution along typical flow paths of the blanket module for $Ha = 4000$ and different Reynolds numbers.

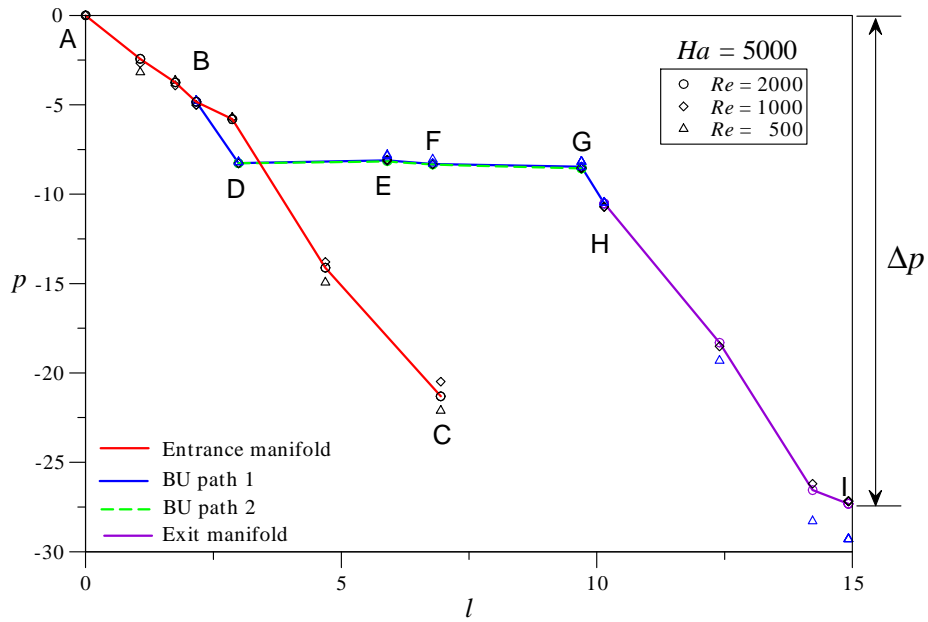


Figure 31: Pressure distribution along typical flow paths of the blanket module for $Ha = 5000$ and different Reynolds numbers.

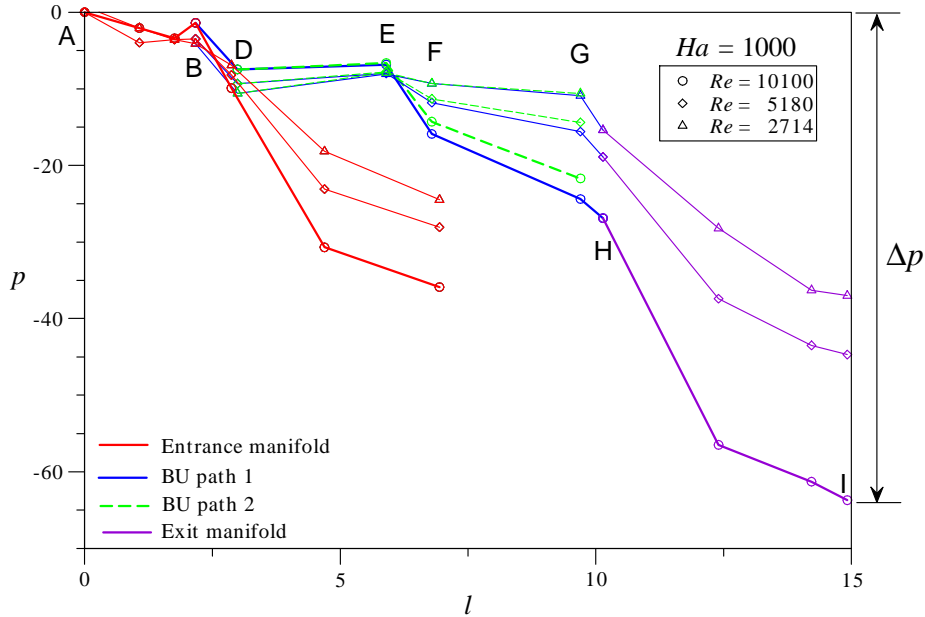


Figure 32: Pressure distribution along typical flow paths of the blanket module for $Ha = 1000$ and different Reynolds numbers. Inertial effects can be clearly identified.

As shown in previous figures the MHD flow through a blanket module requires a total pressure drop Δp between the entrance and the exit of the test section to establish desired flow rates. For strong magnetic fields and moderate flow rates the nondimensional pressure drop approaches a constant value. Inertia effects are present for higher velocities and or for weaker magnetic fields, i.e. for higher Reynolds numbers or for smaller Hartmann numbers. A detailed and systematic analysis of the total pressure drop as a function of Ha and Re has been performed to derive the relevant scaling laws that are required for the layout of the ITER TBM and for extrapolations to a power reactor.

In a first measuring campaign the magnetic field is fixed, i.e. the Hartmann number is adjusted to a defined constant value. Then, for a given Ha , the flow rate is increased and the pressure drop is recorded as a function of the Reynolds number. Results are then combined into a single plot as shown in Fig. 33. One can observe a linear growth of total pressure drop with increasing flow rate, i.e. for larger values of Re . On the other hand the additional inertial pressure drop reduces with increasing magnetic field when the Hartmann number becomes larger.

A similar campaign was performed by keeping the flow rate, given in terms of the Reynolds number, at constant values while varying the magnetic field or the Hartmann number. Results of this series of measurements are displayed in Fig. 34. One observes that the pressure drop approaches monotonically a constant value as Ha is increased. The asymptotic value as $Ha \rightarrow \infty$ corresponds to the pressure drop of an ideally inertialess flow that is dominated explicitly by electromagnetic Lorentz forces. Stronger deviations from inertialess conditions occur for weaker magnetic fields, i.e. smaller Hartmann numbers. Of course inertia effects are stronger expressed for higher Reynolds numbers.

The observed behavior of pressure drop as a function of the Reynolds and Hartmann number,

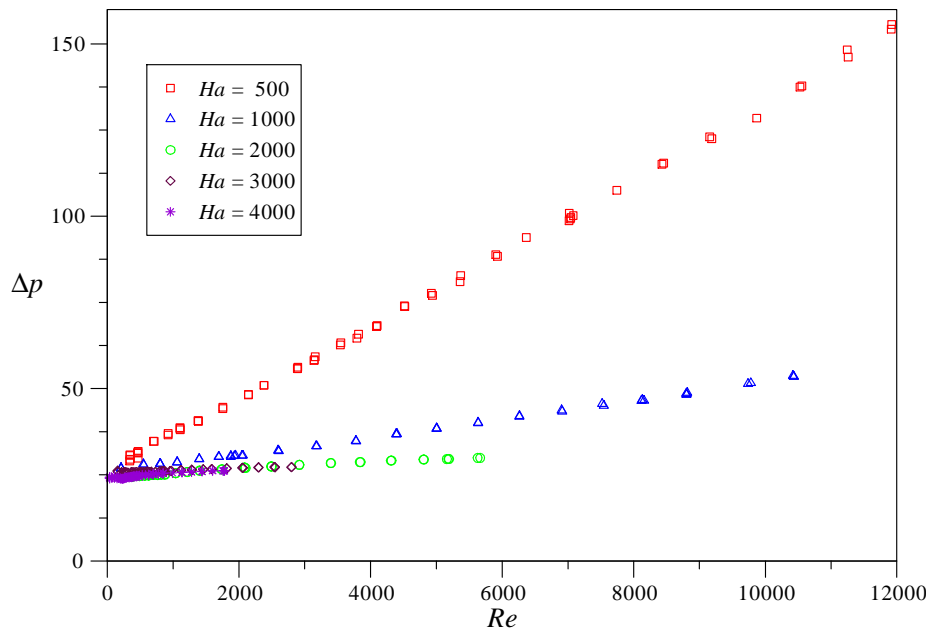


Figure 33: Total pressure drop Δp as a function of the Reynolds number Re for different values of the Hartmann number Ha .

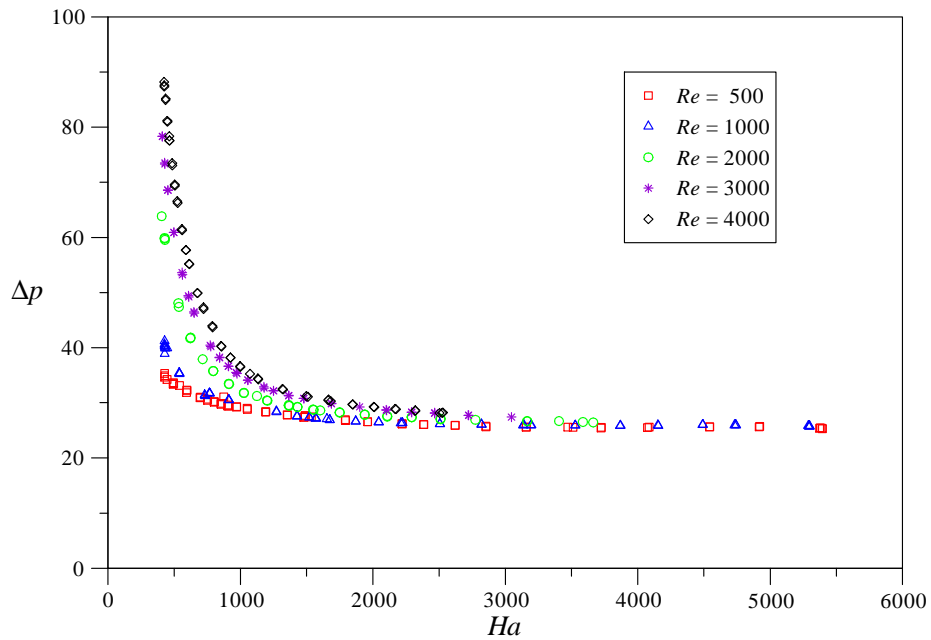


Figure 34: Total pressure drop Δp as a function of the Hartmann number Ha for different values of the Reynolds number Re .

$\Delta p(Re, Ha)$, suggests to look for a suitable representation in form of a pressure drop correlation. It is found that the linear increase of Δp with Re and the strong increase when $Ha \rightarrow 0$ can be modelled as a dependence of a single group, namely the interaction parameter N or better by its reciprocal value as $\Delta p(N^{-1})$. By plotting all the results shown so far in previous Figs. 33, 34 in a single diagram as a function of $N^{-1} = Re/Ha^2$ we find that all measured data points approach closely a straight line that can be used as pressure drop correlation for engineering purposes. These results are displayed in Fig. 35 and for a better visibility of values at high Ha using a log-scale in Fig. 36. The suggested pressure drop correlation then takes the form

$$\Delta p = 25.5 + 2850 N^{-1}. \quad (22)$$

This result is somehow surprising for MHD flows since in previous experiments dealing with single effects like flows in bends or flows in expansions, pressure drop contributions proportional to $Ha^{-1/2}$ or $N^{-1/3}$ were observed (see e.g. Stieglitz, Barleon, Bühler and Molokov (1996) or Bühler and Horanyi (2006)). In those flows the pressure drop was determined by currents flowing in parallel and internal layers of thickness $Ha^{-1/2}$ or $N^{-1/3}$, for the viscous-electromagnetic or the inertial-electromagnetic regimes, respectively. In the present experiment the situation is now completely different. Currents are no longer limited to single layers. They can penetrate through walls into neighboring fluid core regions and create thereby a linear dependence of pressure drop on N^{-1} . Indeed a dependence $\Delta p \sim N^{-1}$ is a strong indication that inertial flows in cores contribute to the present pressure drop correlation.

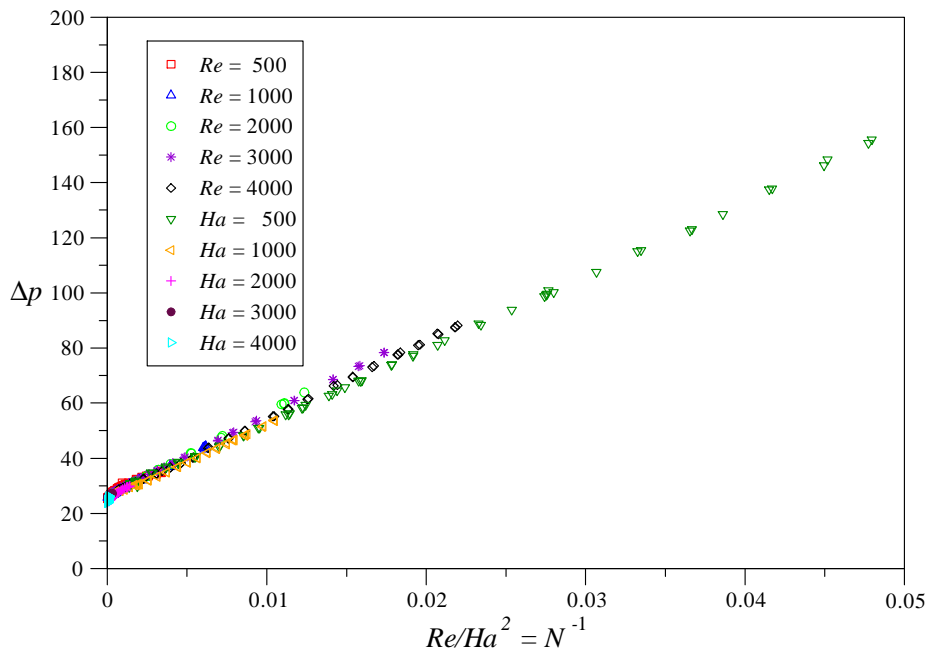


Figure 35: Total pressure drop Δp as a function of N^{-1} for different values of Re and Ha .

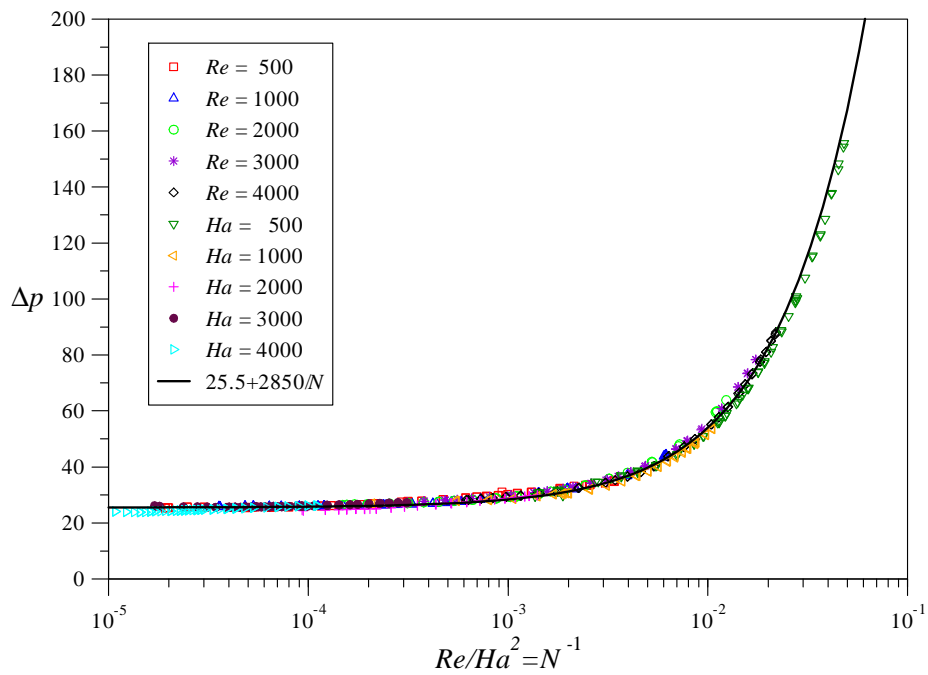


Figure 36: Total pressure drop Δp as a function of N^{-1} for different values of Re and Ha . The logarithmic axis gives better insight for high values of N , i.e. for $N^{-1} \rightarrow 0$. The solid line displays the pressure drop correlation.

5.2 Potential measurements

In a first theoretical attempt the geometry has been decomposed into basic elements for which an asymptotic analysis has been performed. Later the results have been complemented assuming symmetry with respect to grid plates in order to obtain a first idea about the potential distribution on the entire module surface. Such a result is displayed in Fig. 37.

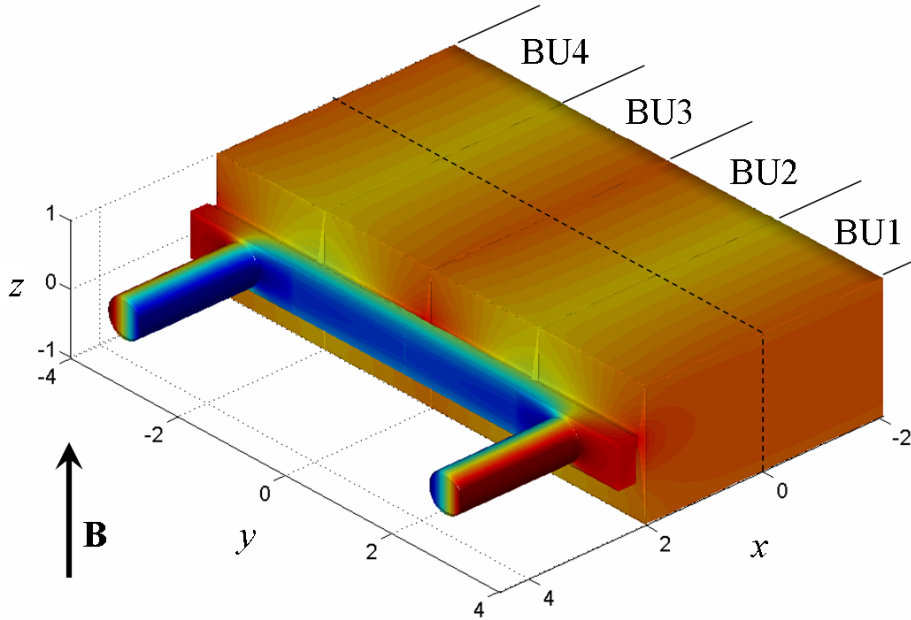


Figure 37: Contours of calculated potential on the surface of the mock-up. Results have been obtained for entrance and exit pipes with poloidal manifold and attached breeder unit. The distribution in the central part has been complemented assuming symmetry conditions for inertialess flows. Cooling plates were not considered here as well as the turning of the flow at the first wall.

As mentioned at the beginning, the surface of the blanket mock-up has been covered by a number of 600 sensors for recording a distribution of wall potential similar to the one shown in Fig. 37. This information is of particular importance since it can be directly compared with theoretical results for validation purposes. Moreover it allows a physical interpretation as an approximate hydrodynamic streamfunction for the flow in the breeder units as outlined in Sect. 4.5. Breeder units BU3 and BU4 are completely instrumented with potential sensors, while BU1 and BU2 have been reserved for pressure measurements. Since it is very likely that the flow behaves almost inertialess for fusion relevant conditions at high interaction parameters N , it is expected that the fluid motion and the potential in BU1 and BU2 can be approximated as symmetric complement. In order to verify this assumption the cross section in the middle plane of the module at $x = 0$ has been completely instrumented over all four BUs along the entire dash line on the Hartmann wall and on both external side walls as shown in Fig. 37.

One result of these potential measurements is shown in Fig. 38. Lines of constant color on the Hartmann wall can be interpreted as hydrodynamic streamlines. We observe that the

flow is well guided towards the first wall due to the presence of the internal cooling plates. Three-dimensional effects are confined to narrow regions close to the first wall and there exists an extended central domain in which the flow seems fully developed. This is an important result which confirms assumptions of a fully developed flow regime used for numerical simulations of the completely electrically coupled system including cooling plates (Mistrangelo (2008)).

The first wall and the external side walls are parallel to the magnetic field and the variation of potential along field lines on these walls gives an information about the flow rate carried by thin jets along these walls. At the first wall we observe some perturbations near the grid plate that separates BU3 and BU4. Here the flow passes through a thin gap that gives also some toroidal restrictions of the flow path at the upper and lower Hartmann walls. Another perturbation is observed at the external side wall close to the back plate. Here we notice a "more red" spot that is caused by the electric coupling with the manifold. In the manifold the velocities and transverse potentials are much higher and the electric connection with the breeder units transfers the larger potentials as electric perturbations near the entrance and exit of the BUs. A similar behavior was already suggested by the simplified model shown in Fig. 37 near $x = 2.$, $y = \pm 4.$

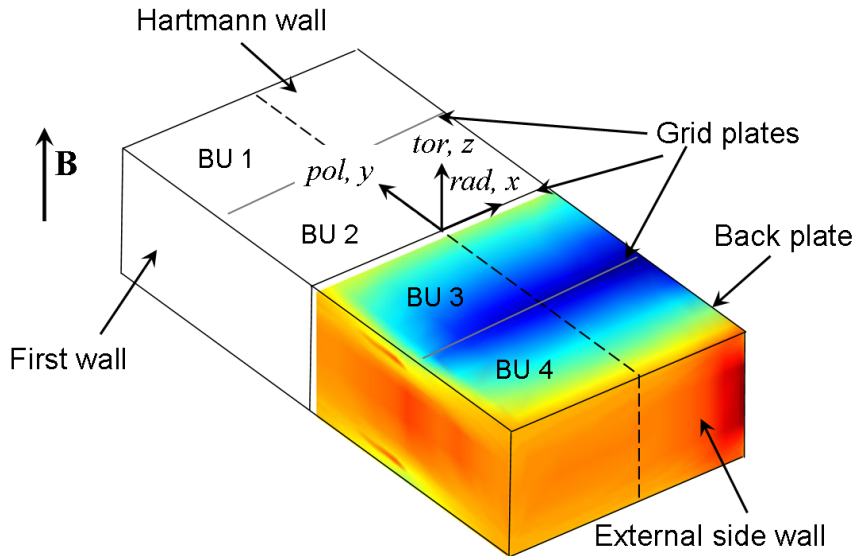


Figure 38: Colored contours of measured surface potential on breeder units BU3 and BU4 for $Ha = 3000$, $N = 1325$.

Although one gets immediately an overall picture of the flow behavior from the potential distribution shown in Fig. 38, more precise information may be seen in the Figs. 39-43 shown below, where potential profiles on the Hartmann wall along the line $x = 0$ are shown. For high Hartmann numbers the potential distribution is almost symmetric with respect to the poloidal center $y = 0$ of the module (see e.g. Fig. 39). This result confirms the weak role of inertia at high values of Ha for moderate Re . Moreover, the distributions in BU1 and BU2 and the ones in BU3 and BU4 show also an approximate symmetry with respect to the grid plates at $y = \pm 2.26$ that separate them. The value at $y = 0$ differs instead by a small amount

from those at the blanket ends. The reason for that is that slightly different high-velocity jets form along the external side walls and along internal grid plates as shown by the numerical analysis (Mistrangelo (2008)). The jets are caused by electric currents flowing inside parallel layers in the direction of the magnetic field. Depending on current density in the walls, toroidal potential distributions establish that determine the flow rate carried by these jets. Internal plates exchange currents with two core regions so that tangential currents in these walls are higher than at the outer ones which communicate only with one flow domain. Therefore jets along internal walls are able to carry higher flow rates than those at external ones, and as a result of that, the flows in cores of inner BUs carry slightly smaller flow rates than those in external BUs. This behavior is reflected in a slightly smaller potential drop across the inner units in comparison with the outer ones.

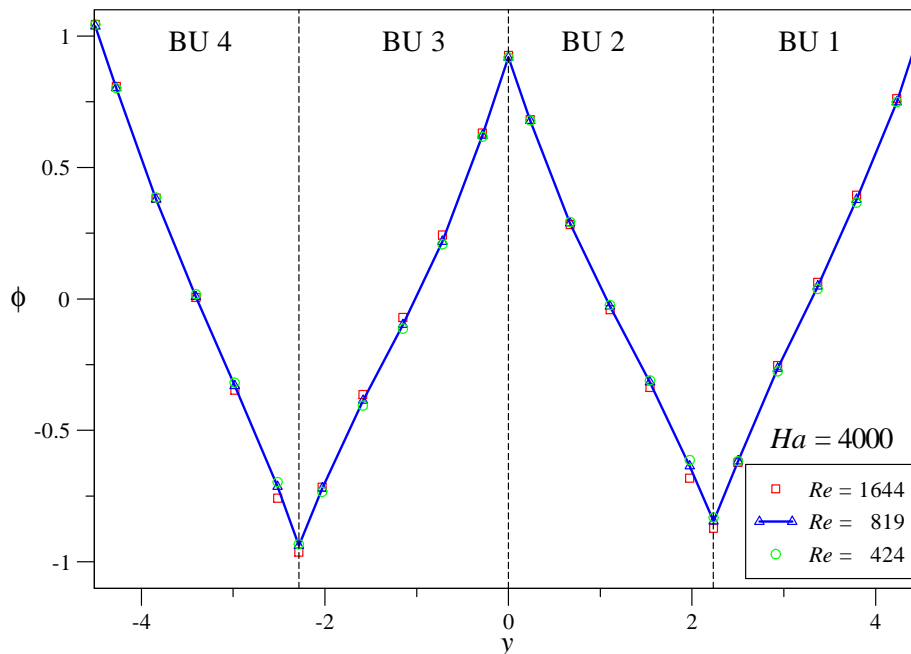


Figure 39: Potential profiles measured along the Hartmann wall of the mock-up at radial position $x = 0$ for $Ha = 4000$ and different Reynolds numbers.

Inertia becomes more important for smaller magnetic fields. For $Ha = 2000$ we observe in Fig. 41 already a deformation of potential profiles, preferentially for the higher Reynolds numbers. The potential minima shift to lower y values for increasing Re and the profiles lose symmetry with respect to the grid plate that separates BU1 and BU2 and the one between BU3 and BU4. For $Ha = 1000$ we see in Fig. 42 an expressed maximum of potential inside BU3 that is even higher than the values at the lateral walls of this unit. This non-symmetric behavior and the formation of a maximum in BU3 become more expressed if we decrease the Hartmann number further to a value $Ha = 500$ as shown in Fig. 43.

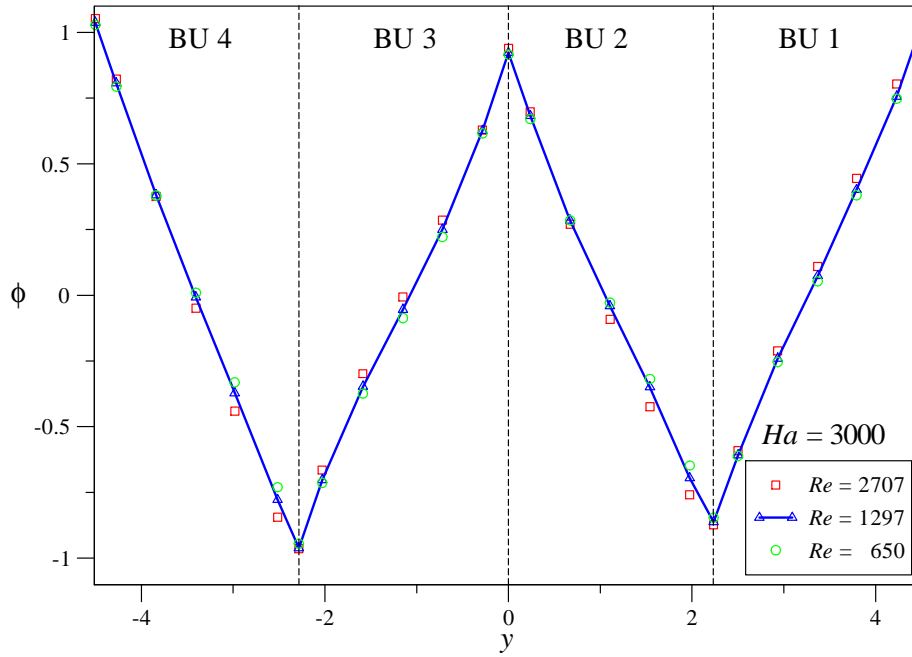


Figure 40: Potential profiles measured along the Hartmann wall of the mock-up at radial position $x = 0$ for $Ha = 3000$ and different Reynolds numbers.

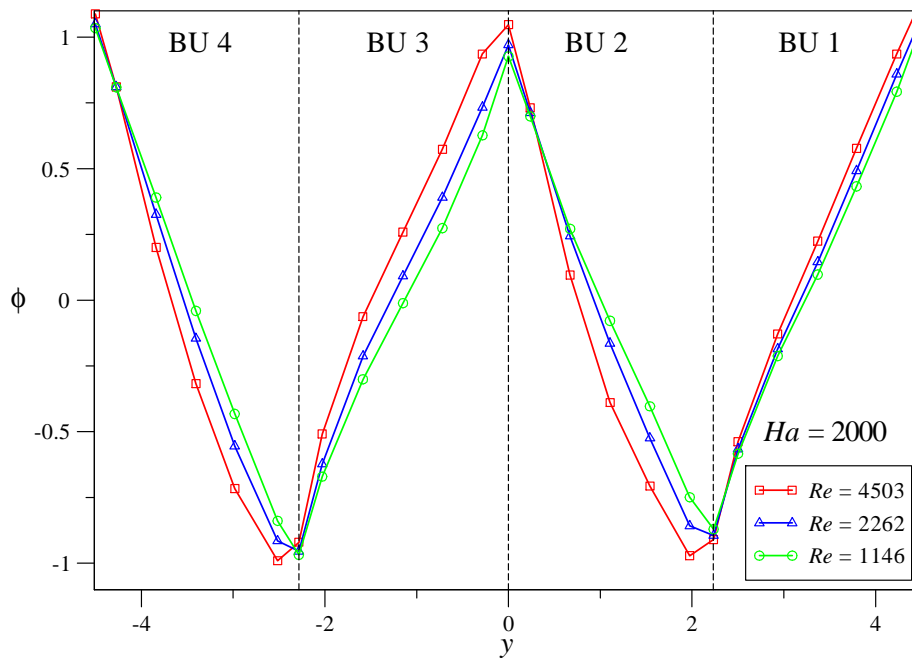


Figure 41: Potential profiles measured along the Hartmann wall of the mock-up at radial position $x = 0$ for $Ha = 2000$ and different Reynolds numbers.

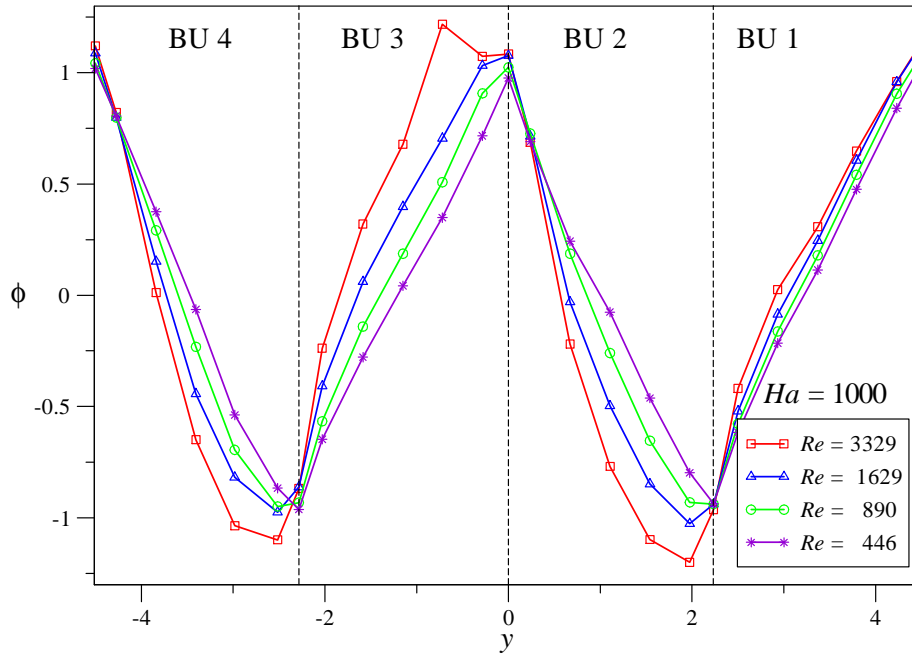


Figure 42: Potential profiles measured along the Hartmann wall of the mock-up at radial position $x = 0$ for $Ha = 1000$ and different Reynolds numbers.

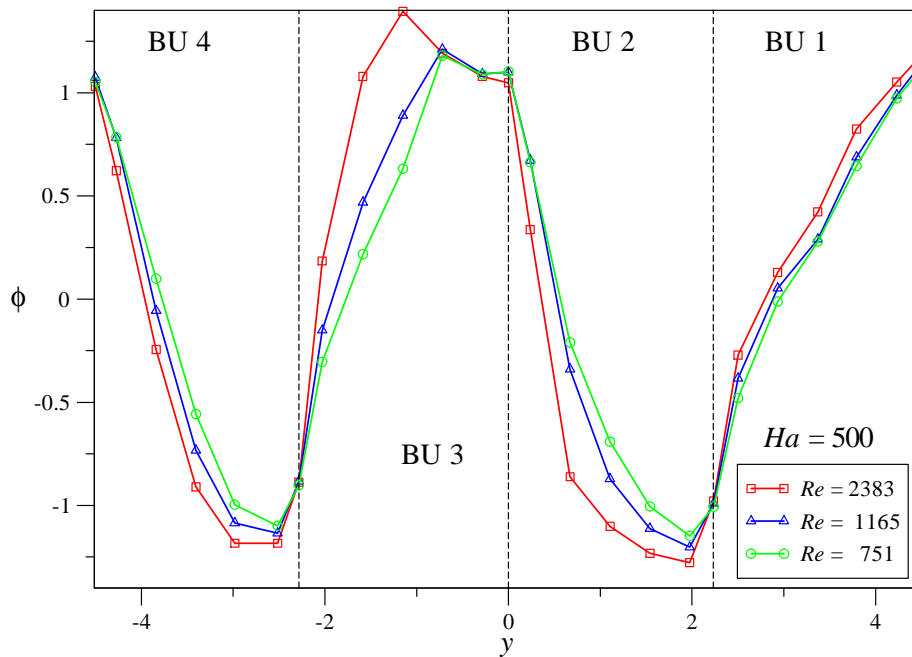


Figure 43: Potential profiles measured along the Hartmann wall of the mock-up at radial position $x = 0$ for $Ha = 500$ and different Reynolds numbers.

5.3 Flow distribution

From the distribution of wall potential we may derive further information for approximate flow rates in single channels formed by the cooling plates or an estimate of mean velocity. According to (21) we have

$$\bar{u} = -\frac{\phi_2 - \phi_1}{y_2 - y_1} = -\frac{\Delta\phi}{\Delta y} \quad (23)$$

as outlined in Sect. 4.5. Results for mean velocity have been obtained by differentiation of potential profiles shown above through Figs. 39-43. For high Hartmann numbers the distribution of flow among sub-channels between cooling plates is not completely uniform. In Figs. 44 and 45 we observe mean velocities that are higher in channels close to grid plates and slightly reduced flow rates in central channels of breeder units. This is in accordance with numerical simulations for an entire cross section of the module at $x = 0$, where also higher fluxes were found along the grid plates. However, the predicted flow in central channels was a bit more uniform than the one we find here (see Mistrangelo (2008)). By reducing the Reynolds number the profiles in BUs become more symmetric. This is a clear indication that inertia has still some effect on the flow, even if it seems from observations of surface potential distribution that the flow in the central part is already fully developed. Most probably inertia effects play a role in distributing the flow into the sub-channels at the entrance to the BUs, at the first wall and at the exit. Once the fluid has reached the sub-channels it flows with a flow rate partly determined by inertial entrance conditions, along the cooling plates in a more or less fully developed manner.

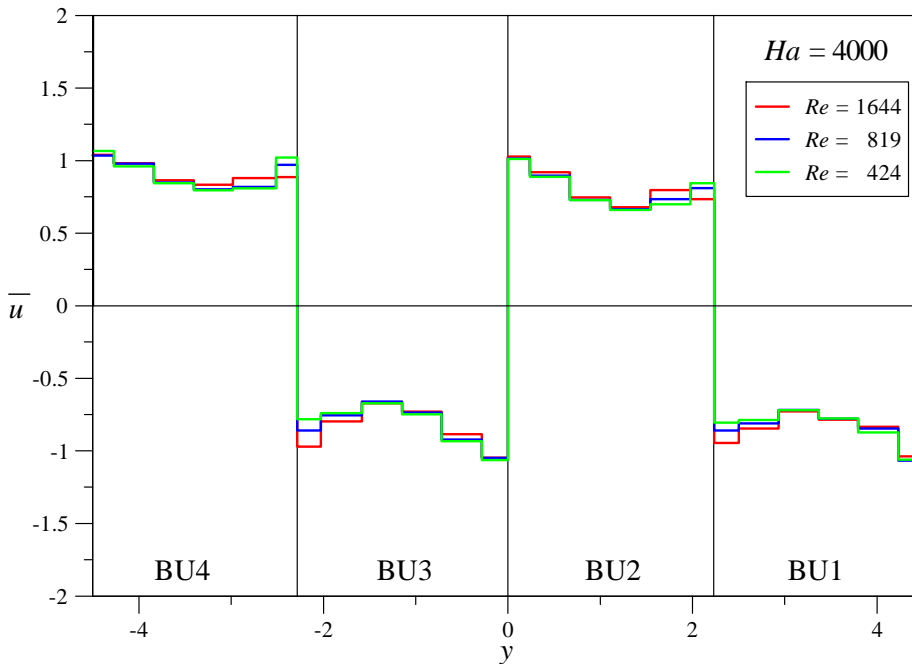


Figure 44: Flow distribution $\bar{u} \approx -\Delta\phi/\Delta y$ in the mock-up at radial position $x = 0$ for $Ha = 4000$ and different Reynolds numbers.

With decreasing Hartmann numbers the flow distribution in BUs becomes progressively inclined and non-symmetric. This behavior can be seen in Figs. 46 and 47 for Hartmann

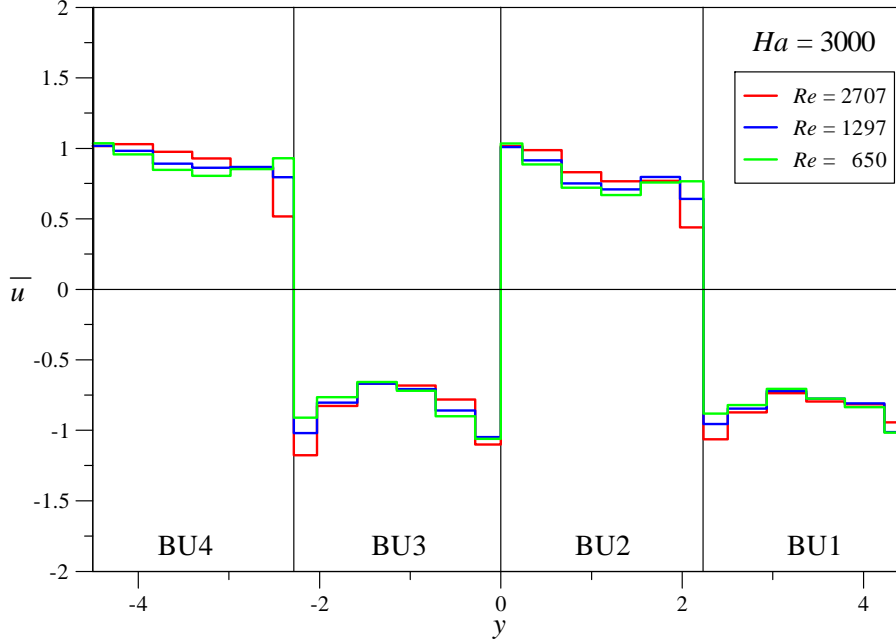


Figure 45: Flow distribution $\bar{u} \approx -\Delta\phi/\Delta y$ in the mock-up at radial position $x = 0$ for $Ha = 3000$ and different Reynolds numbers.

numbers $Ha = 2000$ and $Ha = 1000$. Increasing the Reynolds number leads to a further imbalance of flow between cooling plates. The flow along the first grid plate in BU1 increases strongly with the Reynolds number. A similar behavior is observed in BU3, where the velocity along the left grid plate also increases considerably with Re . The increased flow at the left is balanced by a decreased flux at the right in units BU1 and BU3.

A quite similar trend is also observed in BU2 and BU4. We find also here an increase of flow at the left and a decrease at the right of these units. Moreover, due to the electric coupling the strong flow in BU1 (BU3) tries to pull the weaker neighboring flow in BU2 (BU4) in its own direction. As a result the flow in the right sub-channel of BU2 (BU4) becomes reversed with respect to the main flow carried in this unit.

The behavior described above is even more expressed for the case of a moderate Hartmann number of $Ha = 500$ as shown in Fig. 48. For this Hartmann number we observe even a reversed flow in 3 sub-channels of BU3. One can clearly see from the figure that the effects are caused primarily by inertia, since reducing Re tends to reestablish more uniform conditions.

Results displayed so far have been illustrated in Fig. 49 for $Ha = 4000$, 1000 and 500 . For $Ha = 4000$ the flow paths are as foreseen in the design. We find a flow towards the first wall in BU1 and BU3 and a flow towards the back plate in BU2 and BU4. For $Ha = 1000$ we observe closed recirculation loops in BU2, BU3 and BU4. The magnitude of reversed flow and the regions in which it occurs increase further for smaller Ha and for higher Re as shown in Fig. 49 for $Ha = 500$.

Closed recirculation loops could cause a safety problem in a fusion blanket, since in these regions there exists the possibility for tritium accumulation. For strong magnetic fields as foreseen in ITER, where Ha may even exceed values of 10^4 , however, such regions seem not to

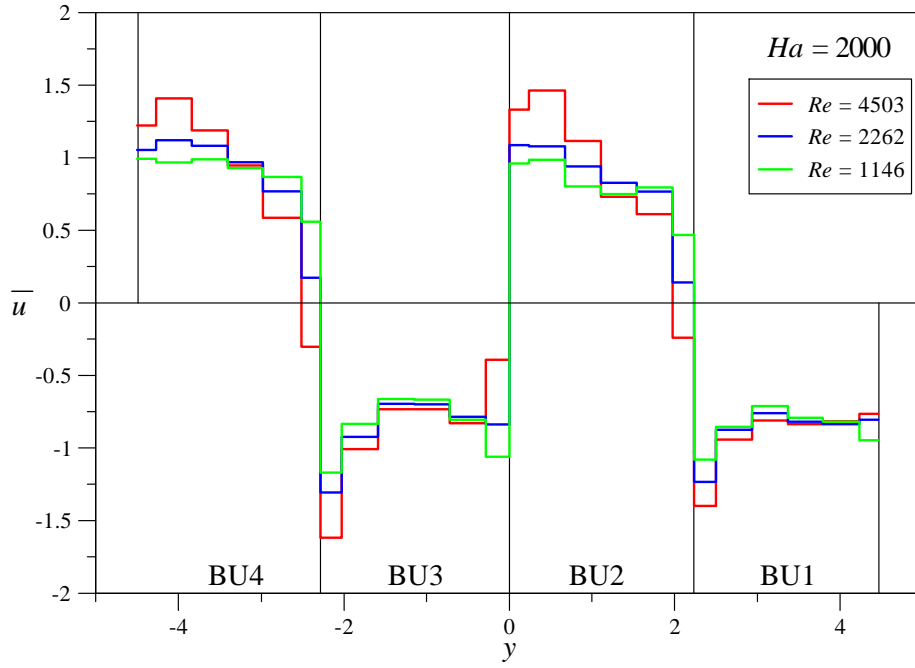


Figure 46: Flow distribution $\bar{u} \approx -\Delta\phi/\Delta y$ in the mock-up at radial position $x = 0$ for $Ha = 2000$ and different Reynolds numbers.

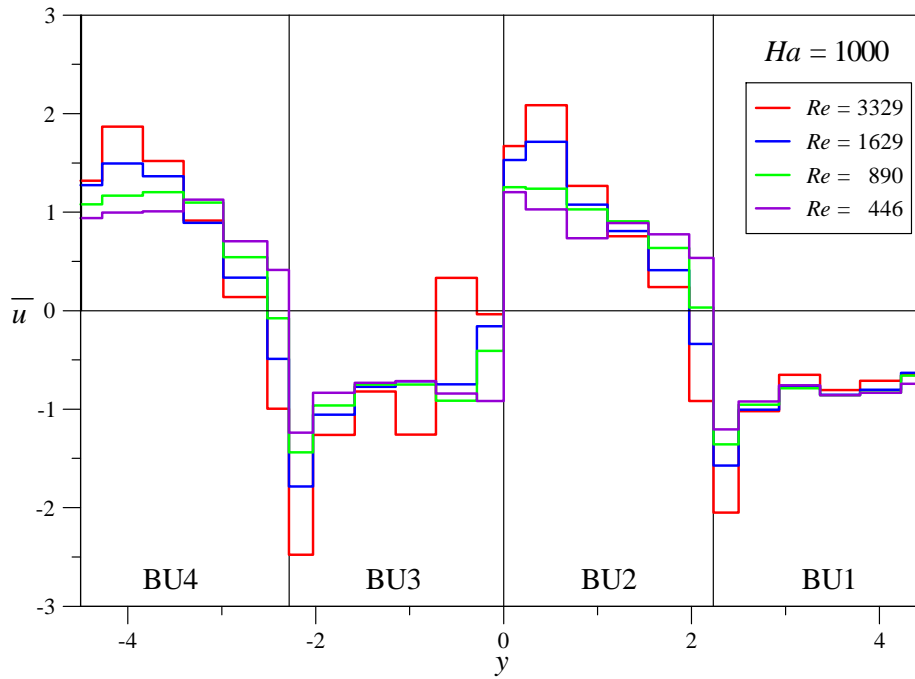


Figure 47: Flow distribution $\bar{u} \approx -\Delta\phi/\Delta y$ in the mock-up at radial position $x = 0$ for $Ha = 1000$ and different Reynolds numbers.

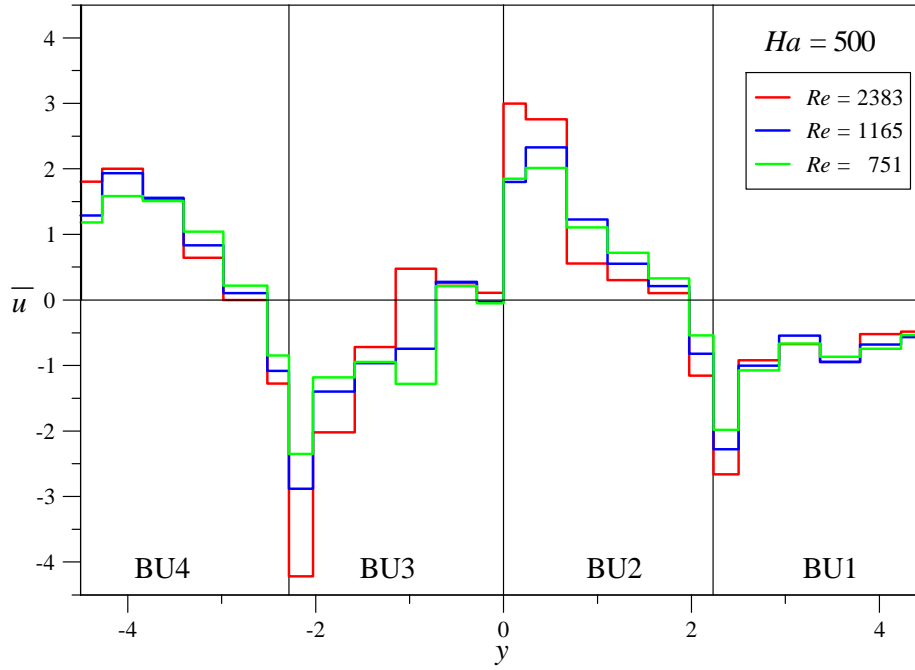


Figure 48: Flow distribution $\bar{u} \approx -\Delta\phi/\Delta y$ in the mock-up at radial position $x = 0$ for $Ha = 500$ and different Reynolds numbers.

exist according to present experiments. As a summary of these considerations we may conclude that for fusion conditions, where Hartmann numbers are very high, the flow in breeder units follows the paths as foreseen in the design. The small Reynolds numbers favor a more uniform flow balance between BUs, even if for the values of parameters realized in the experiments a perfect equi-partitioning was not completely achieved.

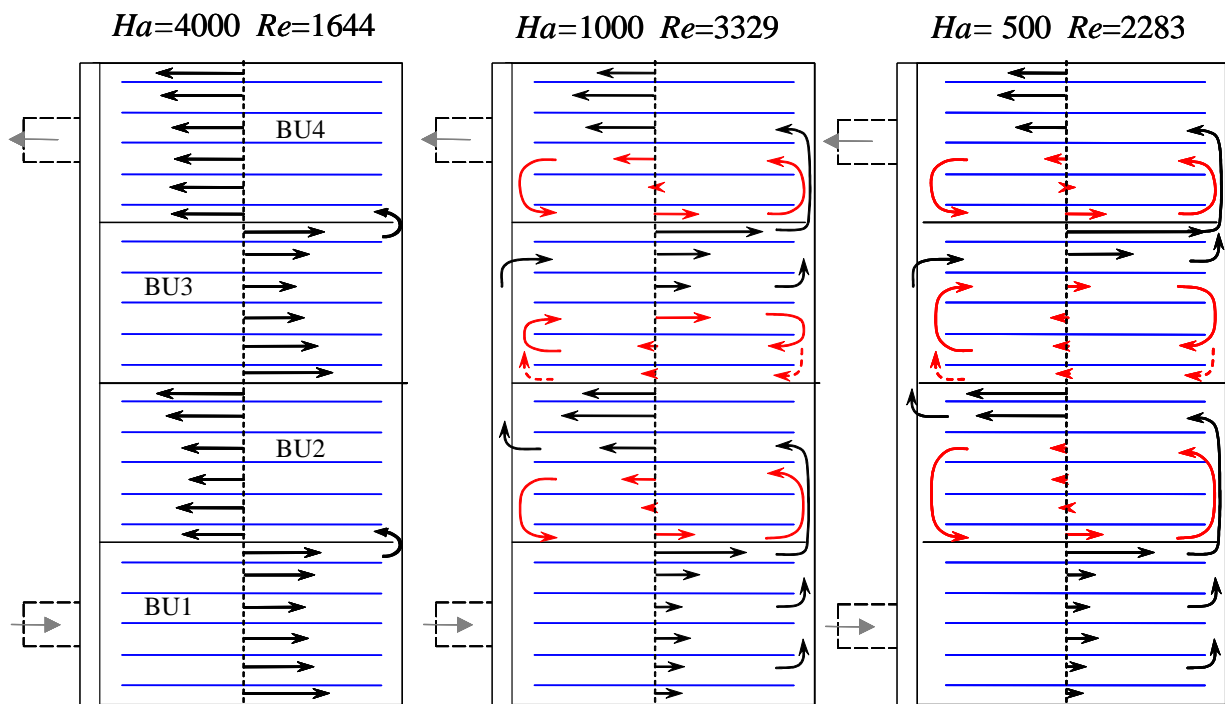


Figure 49: Sketch of flow paths in breeder units according to mean velocities derived through Figs. 44-48. Contributions marked in red indicate closed recirculation loops involving reversed velocities in comparison to the main flow direction in the BUs. They are driven by inertia and electromagnetic coupling.

5.4 Extrapolation to ITER TBM conditions

Results presented through previous sections support the assumption that MHD flows in breeder units of an ITER test blanket module are most likely inertialess and governed by a balance between pressure forces and Lorentz forces. The pressure distribution along the module has been measured for the present scaled mock-up using NaK as a model fluid. The results can be summarized as shown in Fig. 50. This figure has been complemented with respect to Fig. 29 by the flow contributions in units BU3 and BU4 assuming symmetry as indicated in the plot.

We can identify contributions Δp_E when the flow passes through the circular entrance pipe and expands into the manifold. We have to account for this contribution twice, at the entrance and when the flow from the second poloidal manifold is collected in the exit pipe. In the module itself we find a total pressure drop $\Delta p_{BU,M}$. It is composed by the part Δp_{BU} that occurs when fluid passes into the breeder units, flows along the units to the first wall where it turns by 180° , flows back in the next unit and passes through the thin gap in the back plate into the draining manifold. The remaining fraction is caused by the flow in the manifolds and it is called here $\Delta p_M = \Delta p_{BU,M} - \Delta p_{BU}$.

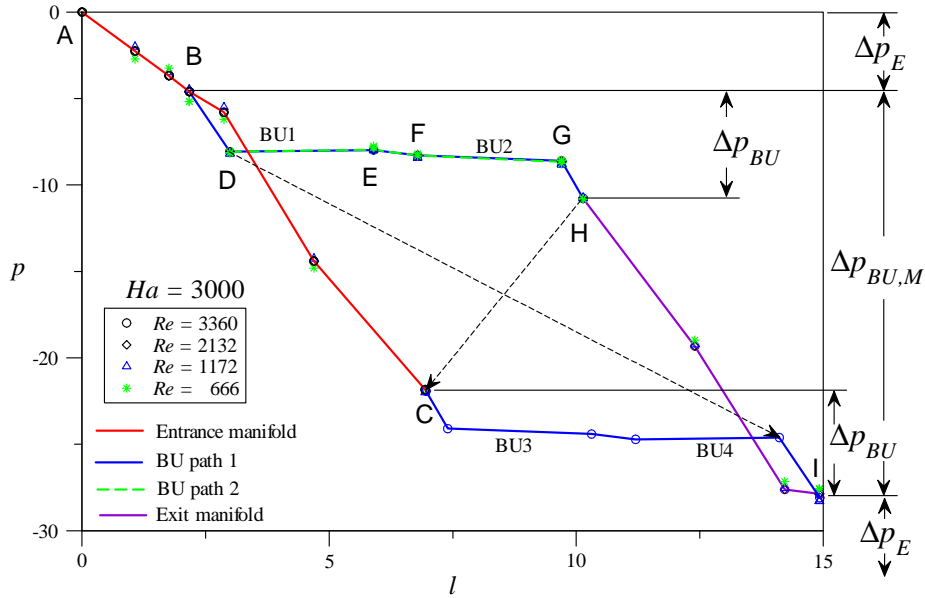


Figure 50: Pressure drop contributions in the mock-up. Δp_E - entrance / exit pipes and connection with manifolds, $\Delta p_{BU,M}$ - breeder units and manifold, Δp_{BU} - breeder units.

The present MHD mock-up is composed by 4 BUs. The TBM in ITER, however consists of 8 breeder boxes that are fed and drained by the same type of manifold. As a result the velocity in the access tube and manifold is twice as large as the one considered here, since these channels now have to feed other 4 BUs. This gives rise to twice the pressure drop as that measured in the present experiment along flow paths AC and HJ. Moreover, the flow in the manifolds has to pass along a poloidal length that is twice as long since now the blanket module is formed by 8 units instead of 4 used in the mock-up experiment. For that reason we have to add another $2\Delta p_M$ to the total balance. Finally we obtain the nondimensional pressure distribution of a

TBM with 8 BUs as shown in Fig. 51. The total pressure drop evaluates as

$$\Delta p_{8BU} = 4\Delta p_E + 2\Delta p_M + \Delta p_{BU} + 2\Delta p_M \approx 93. \quad (24)$$

As shown in Sect. 2 the pressure drop can be expressed as

$$\Delta p = \frac{c}{1+c} A. \quad (25)$$

In general A is a function of Ha and Re . It has been shown above that A depends for the present problem only on the single nondimensional group N and its magnitude becomes constant as $N \rightarrow \infty$ as expected in ITER. The nondimensional pressure drop for the ITER TBM then evaluates as

$$\Delta p_{ITER} = \frac{\left(\frac{c}{1+c}\right)_{ITER}}{\left(\frac{c}{1+c}\right)_{mock-up}} \Delta p_{8BU}, \quad (26)$$

where temperature-dependent material properties have been used for PbLi and Eurofer at 500 °C in ITER and for NaK and stainless steel at 50 °C in the present experiment (see Jauch et al. (1986), Foust (1972), Stahl-Eisen-Werkstoffblätter (1992), Tavassoli (2002)) to calculate the wall conductance ratios. As a result we obtain

$$\Delta p_{ITER} = 3.1 \Delta p_{8BU} = 288. \quad (27)$$

For an average velocity of $v_0 = 0.001$ m/s in breeder units, a magnetic field of $B_0 = 6$ T, and a Hartmann length (half toroidal dimension) of a breeder unit of $L = 0.09$ m we find the result that a dimensional pressure difference of

$$\Delta p^* = \sigma_{PbLi} v_0 L B_0^2 \Delta p_{ITER} = 0.69 \text{ MPa} \quad (28)$$

is required to drive the flow at desired flow rates. This value seems acceptable for the operation of a TBM in ITER, even if it appears to be relatively high considering the small velocities in breeder units. It represents to our best knowledge a conservative estimate since it has been derived using the wall conductance ratios c_{ITER} and $c_{mock-up}$ taken for the breeder units. Nevertheless, the major fraction of pressure drop occurs in feeding and draining pipes and in poloidal manifolds, where the wall conductance parameters based on the dimensions of these elements are a bit higher. If we evaluate (26) with values of c based on dimensions of feeding pipes and manifolds we obtain a slightly smaller result i.e.

$$\Delta p_{ITER} = 0.62 \text{ MPa}. \quad (29)$$

In addition to that, the liquid metal velocities in feeding and draining pipes and in poloidal manifolds are higher than in the breeder units. Therefore a reduction of pressure drop with respect to present results should be possible by using larger cross-sections in these geometric elements. This could be useful for studying flow regimes which allow faster exchange of the fluid in order to keep the tritium content in the blanket as small as possible.

It should be also mentioned that in a recent publication by Mergia and Boukos (2008) the given electric conductivity of Eurofer is about 15% lower than the one by Tavassoli (2002). This fact would reduce the pressure drop roughly by the same percentage compared with (28).

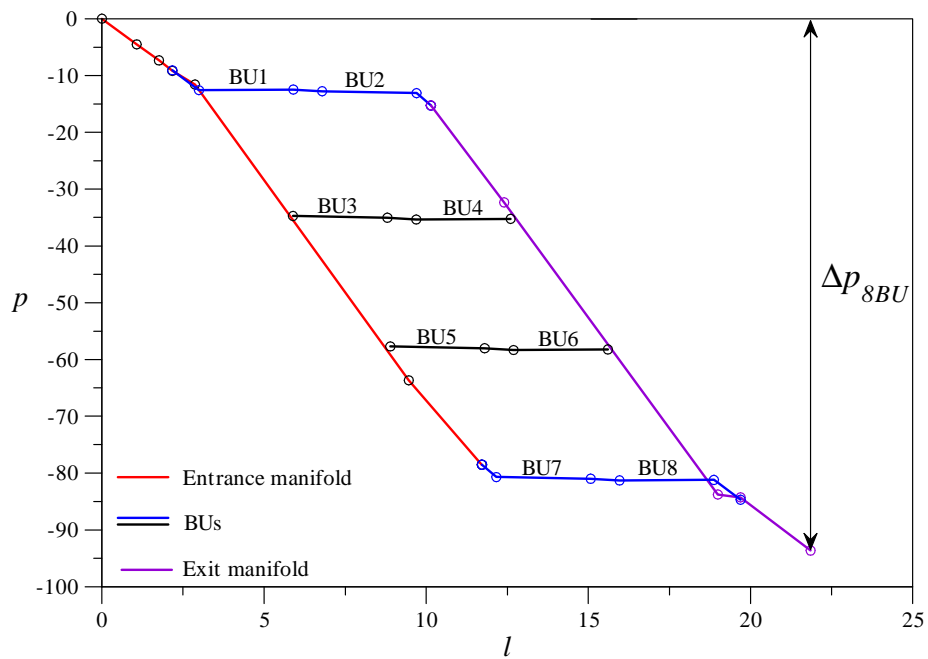


Figure 51: Pressure distribution for a TBM geometry with 8 BUs. Results have been obtained by extrapolation of measurements in a test section with 4 BUs.

6 Conclusions

Liquid metal magnetohydrodynamic flows in a scaled mock-up of a helium cooled liquid metal TBM for ITER have been investigated experimentally in the MEKKA laboratory of the Forschungszentrum Karlsruhe. At present day the fluid domains in the complicated three-dimensional structure of the module with large number of cooling plates, expansions, contractions etc. are far from being properly resolved with required numerical grids on available computers. Moreover, electric currents are able to cross conducting walls and interact with neighboring fluid domains, creating strong electromagnetic flow coupling among channels inside breeder units. The purpose of the experiments is to provide a data base for validation of existing numerical tools for simulations of such kind of flows and for validation of new predictive tools with extended capabilities to be developed during the next years. While a full 3D numerical solution of the problem is presently not available for very strong magnetic fields, the experimental data obtained in this campaign define the scaling laws which are required for the development of a reliable test blanket for ITER and for an extrapolation of results to a DEMO reactor.

The experimental mock-up has been build according to a design developed at CEA for a HCLL test blanket module (Rampal et al. (2005), Rampal et al. (2006)), scaled down by a factor of 2 to fit into the magnet available in the MEKKA laboratory. The test section was installed into the liquid metal loop using NaK as a model fluid. The experiment was fitted with 27 pressure taps for recording pressure distribution along typical flow paths. Moreover the surface of the mock-up has been covered by insulating plates that carry about 600 sensors for detection of electric potential on the walls. Surface potentials can be directly compared with theoretical predictions for code validation purposes, but they also serve as approximate hydrodynamic streamfunction of the flow.

In accordance with previous theoretical predictions the major part of pressure drop appears in the entrance pipes and poloidal manifolds. The cross-sections of these elements are relatively small in comparison with those in breeder units. As a consequence the velocities here are higher, which leads to the observed large contribution to pressure drop in these geometries. Additional but smaller contributions are present when the flow passes through narrow gaps in the back plate or at the first wall. The pressure drop in breeder units, where velocities of the order of 1–2 mm/s are foreseen, is negligible in comparison with the other contributions. It is found that the pressure drop scales proportionally to the square of the magnetic field B_0 and linearly with the average velocity v_0 in the inertialess flow regime, i.e. for small Reynolds numbers Re . With increasing Re the pressure drop increases further due to inertia effects in 3D elements of the module. It has been found that this additional inertial contribution depends on the interaction parameter N that characterizes the ratio of electromagnetic to inertia forces. Finally a pressure drop correlation of the form

$$\Delta p = 25.5 + 2850 N^{-1} \quad (30)$$

has been derived in which the nondimensional quantity Δp stands for the total pressure drop scaled by $\sigma v_0 L B_0^2$, where σ denotes the electric conductivity of the used model fluid NaK and L is a typical length scale of the problem.

Results have been extrapolated to ITER conditions where the fluid is PbLi and magnetic fields are higher. From the present experiments we can conclude that for ITER conditions the pressure drop in the module is most likely inertialess. Estimates for the considered geometry suggest a total pressure drop over the module of about $\Delta p^* = 0.69$ MPa for a magnetic field of

$B_0 = 6$ T and a velocity in breeder units of $v_0 = 1$ mm/s. This value appears to be relatively high considering the small velocities in breeder units. On the other hand it seems still acceptable. In the present design the major fraction of pressure drop occurs in feeding and draining pipes and in poloidal manifolds, where the liquid metal velocities are higher than in the breeder units. A reduction of pressure drop with respect to present results should be possible by using larger cross-sections in these geometric elements of the blanket or by using some electrical insulation in the supplying piping system and manifolds.

Results for electric potential measurements on the surface of the module yield information about flow distribution between the cooling plates. It has been found that the flow behaves almost as foreseen in the design. We observe flows towards the first wall in all sub-channels of breeder units with odd numbers and returning flows towards the back plate in units with even numbers. Near grid plates the velocity is higher than in the central part of the breeder units as predicted in numerical simulations (Mistrangelo and Bühler (2008)). The flow in the central channels still shows a small deformation of velocity profiles that was not predicted by the calculations. A reason for this slight disagreement could be that in the experiments still some weak influence of inertia is present at locations where the flow is distributed into the sub-channels. In the simulations instead a perfectly developed flow regime has been assumed, where inertia effects do not contribute to the results. Nevertheless, the agreement seems quite satisfactory considering the very complicated geometry for which calculations in a central cross section have been performed taking into account the full electromagnetic coupling.

Inertia effects become well expressed for smaller magnetic fields, i.e. for lower Hartmann numbers Ha . For such conditions the flow distributions in breeder units become non-symmetric and regions with even reversed flow could appear in comparison with the main flow directions in the breeder units. Reversed flows are associated with closed recirculation loops in which tritium could accumulate. However, recirculations have been observed only for magnetic fields or Hartmann numbers smaller than in ITER operation. Since for ITER and also for DEMO conditions inertia effects do not play a significant role in a helium cooled liquid-metal blanket the flow will be as foreseen in the concept and recirculation loops will not occur for the present design.

Experiments have been performed under the assumption that the magnetic field over the whole TBM is constant. In a Tokamak, however, the magnetic field varies slightly with the radial coordinate. As a result of that additional pressure drop and unknown flow distribution have to be expected. This point will be investigated using the present experimental mock-up in an upcoming new experimental campaign.

The experimental mock-up has been built according to the CEA-design as published by Rampal et al. (2005). In the meantime the concept has been modified. The present design contains only 3 cooling plates per breeder unit. This fact should facilitate numerical calculations since the number of near-wall layers and coupled regions that have to be resolved is now smaller. On the other hand substantial changes of the flow paths at the first wall have been introduced to ensure the mechanical integrity of the blanket during accidental overpressure. The gap through which the liquid metal passes from one unit into the other is now divided in several relatively small openings with large changes of cross-section measured along magnetic field lines. Contractions of this type are known to create considerable additional MHD pressure drop with significant influence on the flow pattern. As a consequence we have to expect strongly increased pressure drop at this position, where it was only marginal in the first design. The entrance into

the breeder units has been also modified. In the current concept the space initially foreseen for poloidal distribution of the flow has been omitted. This could have a negative impact on equi-partitioning of the flow between the cooling plates. These points should be considered in more detail in future research programs. Moreover, internal structures of walls due to the presence of helium channels create non-uniform and anisotropic conductance of the walls that couple electrically neighboring fluid domains. This point which has been ignored in the present investigation should be taken into account as well.

In the present experimental campaign only one column of breeder units has been considered. In the ITER TBM or in DEMO applications multiple columns are connected to single supplying and draining lines through additional toroidal manifolds. These latter ones have not been considered in very detail in the past. The limited knowledge in this field requires also further investigations in future.

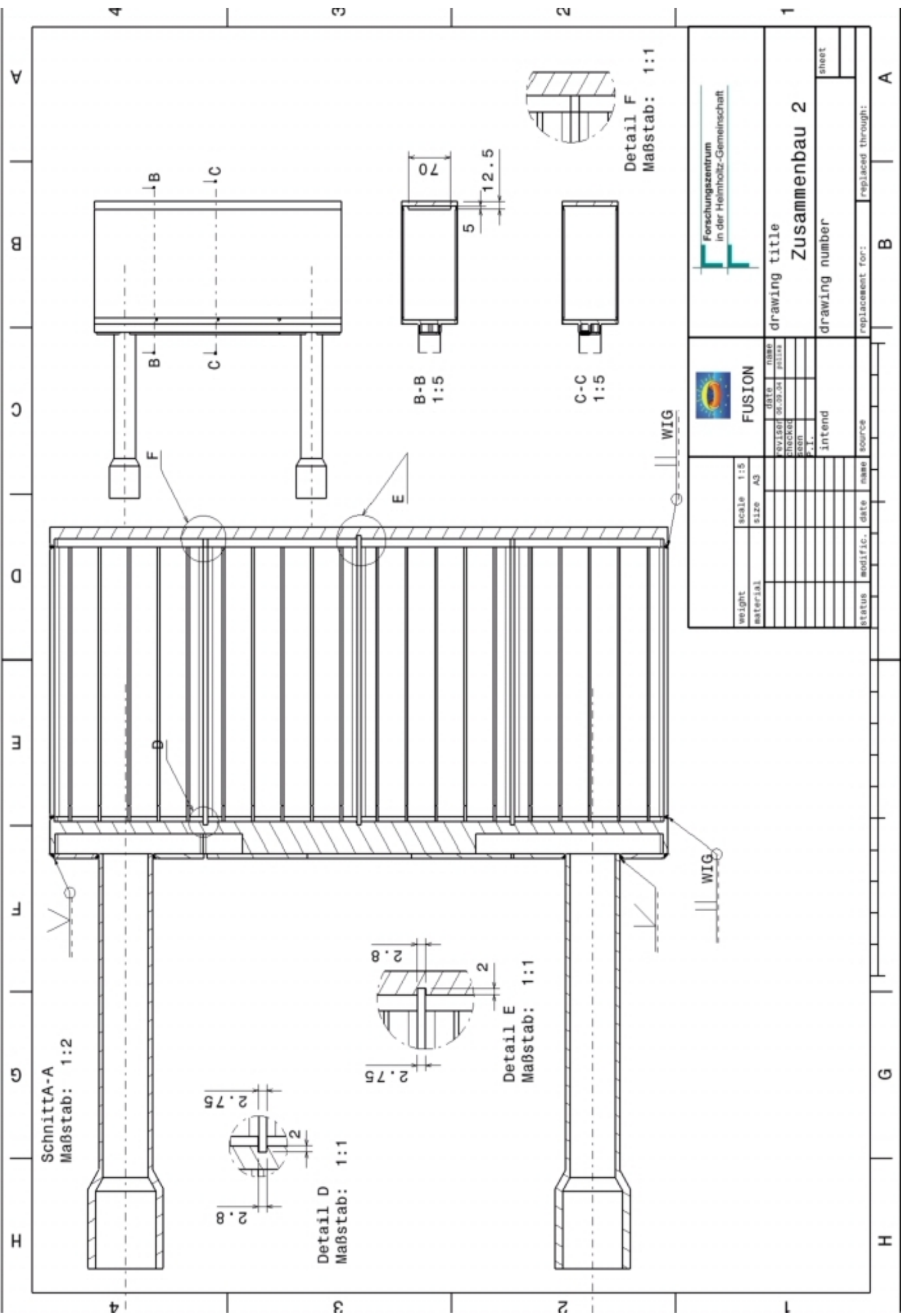
References

- Barleon, L., Mack, K.-J. and Stieglitz, R.: 1996, The MEKKA-facility - A flexible tool to investigate MHD-flow phenomena, *Technical Report FZKA 5821*, Forschungszentrum Karlsruhe.
- Bühler, L.: 1995, Magnetohydrodynamic flows in arbitrary geometries in strong, nonuniform magnetic fields, *Fusion Technology* **27**, 3–24.
- Bühler, L.: 1998, Laminar buoyant magnetohydrodynamic flow in vertical rectangular ducts, *Physics of Fluids* **10**(1), 223–236.
- Bühler, L.: 2005, Magnetohydrodynamic pressure-driven flows in the HCLL blanket, *Fusion Engineering and Design* **75-79**, 923–926.
- Bühler, L.: 2008, Three-dimensional liquid metal flows in strong magnetic fields, *Technical Report FZKA 7412*, Forschungszentrum Karlsruhe. Habilitationsschrift Universität Karlsruhe.
- Bühler, L. and Horanyi, S.: 2006, Experimental investigations of MHD flows in a sudden expansion, *Technical Report FZKA 7245*, Forschungszentrum Karlsruhe.
- Bühler, L. and Molokov, S.: 1994, Magnetohydrodynamic flows in ducts with insulating coatings, *Magnetohydrodynamics* **30**(4), 439–447.
- Bühler, L. and Wetzel, C.: 2006, Asymptotic analysis of 3D buoyant magnetohydrodynamic flows in strong magnetic fields, *Magnetohydrodynamics* **42**(2-3), 3–7.
- Foust, O. J.: 1972, *Sodium - NaK engineering handbook*, Gordon and Breach Science Publishers.
- Jauch, U., Karcher, V., Schulz, B. and Haase, G.: 1986, Thermophysical properties in the system Li-Pb, *Technical Report KfK 4144*, Kernforschungszentrum Karlsruhe.
- Kharicha, A., Molokov, S., Aleksandrova, S. and Bühler, L.: 2004, Buoyant convection in the HCLL blanket in a strong uniform magnetic field, *Technical Report FZKA 6959*, Forschungszentrum Karlsruhe.
- Mergia, K. and Boukos, N.: 2008, Structural, thermal, electrical and magnetic properties of Eurofer 97 steel, *Journal of Nuclear Materials* **373**, 1–8.
- Mistrangelo, C.: 2008, Magnetohydrodynamic flow in a mock up of a HCLL blanket. Part I Numerical analysis, *Technical Report FZKA 7312*, Forschungszentrum Karlsruhe.
- Mistrangelo, C. and Bühler, L.: 2008, Electric flow coupling in the HCLL blanket concept, *Fusion Engineering and Design to be published*.
- Molokov, S.: 1995, Liquid metal flows in insulating elements of self-cooled blankets, *Fusion Engineering and Design* **27**, 642–649.
- Müller, U. and Bühler, L.: 2001, *Magnetofluidynamics in Channels and Containers*, Springer, Wien, New York. ISBN 3-540-41253-0.

- Rampal, G., Gatelet, D., Giancarli, L., Laffont, G., Li-Puma, A., Salavy, J. and Rigal, E.: 2006, Design approach for the main ITER test blanket modules for the EU helium cooled lithium-lead blankets, *Fusion Engineering and Design* **81**, 695–700.
- Rampal, G., Li-Puma, A., Poitevin, Y., Rigal, E., Szczepanski, J. and Boudot, C.: 2005, HCLL TBM for ITER - design studies, *Fusion Engineering and Design* **75-79**, 917–922.
- Stahl-Eisen-Werkstoffblätter: 1992, *Physikalische Eigenschaften von Stählen*, Verein Deutscher Eisenhüttenleute.
- Stieglitz, R., Barleon, L., Bühler, L. and Molokov, S.: 1996, Magnetohydrodynamic flow through a right-angle bend in a strong magnetic field, *Journal of Fluid Mechanics* **326**, 91–123.
- Tavassoli, F.: 2002, DEMO interim structural design criteria. Appendix A Material Design Limit Data A3.S18E EUROFER steel, *Technical Report CEA/DEN/SAC/DMN D0-155-21/06/02*, Commissariat à l’Energie Atomique.

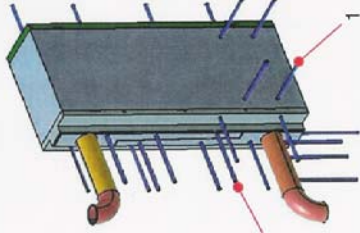
A Appendix

Some details of the design and pre testing of the TBM module are shown through the design drawings and figures in this appendix.



		drawing title Zusammenbau 2	
drawing number		sheet	
weight material	scale 1:5 size A3	status modify. date name source	replace for:
FUSION		intend	
DATE REVISION CHECKED SEEN	NAME P11111	replaced through:	

Druckgerät: HCLL Mock Up M1:2
 Herkunft: Fertigung BTI-F
Betriebsdaten + Klassifizierung:
 Gesamtvolumen: 9,74l (incl. Rohranschlüssen)
 Betriebsmedium: NaK (eut., Schmelzpkt. -12°C)
 FluidEinstufung: Gruppe 1 (entflammbar, hochentzündlich)
 Betriebsdruck PS: 5,6 bar / Vakuum
 PS x Vges.: 54,54 damit Behälter nach Art.3 Abs. 3 DGR 97/23/EG
 Betriebstemp T_B: RT
 Klassifizierung Art10 DGR: - entfällt
 Notw. Konformitätsbewertung: - entfällt
 Betriebsort: Nur MEKKA Labor IKET B274



Druckprüfung Dichtheitsprüfung Vakuumtest

1. Prüfbereich:

1.1 Leckagevorprüfung

2. Prüfvorschrift

Spezifikation: AD 2000 Sonstige:

3. Prüfdaten für Überdrucktest:

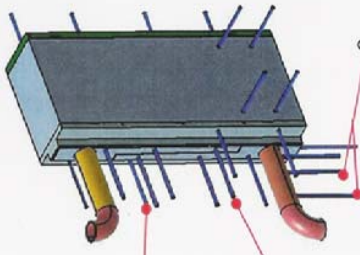
Prüffaktor F_p: entfällt
 Prüfdruck P_p[bar]: 1,5
 Prüftemperatur T_p[°C]: RT
 Tag der Prüfung: 09.11.2005

6. Bemerkungen/Abweichungen/Skizze:

- Behälter mittels wässriger Seifenlauge benetzt und visueller Leckagetest durchgeführt.
 7. Prüfbefunde:
 - geringe Gasblasenbildung an Swagelocküberwurfmutter Pos.1 feststellbar. (Mutter nachgezogen!)
 - Druckanzeige blieb beständig. Keine Leckagen an Schweißnähten feststellbar.

.....FKZ-IKET, den 09.11.2005..... entfällt.....
 Ort, Datum
J.Rey.....
 Name (leserlich), Unterschrift (Prüfer) ggljs. Name (leserlich), Unterschrift (Betreiber)

Druckgerät: HCLL Mock Up M1:2
 Herkunft: Fertigung BTI-F
Betriebsdaten + Klassifizierung:
 Gesamtvolumen: 9,74l (incl. Rohranschlüssen)
 Betriebsmedium: NaK (eut., Schmelzpkt. -12°C)
 FluidEinstufung: Gruppe 1 (entflammbar, hochentzündlich)
 Betriebsdruck PS: 5,6 bar / Vakuum
 PS x Vges.: 54,54 damit Behälter nach Art.3 Abs. 3 DGR 97/23/EG
 Betriebstemp T_B: RT
 Klassifizierung Art10 DGR: - entfällt
 Notw. Konformitätsbewertung: - entfällt
 Betriebsort: Nur MEKKA Labor IKET B274



Druckprüfung Dichtheitsprüfung Vakuumtest

1. Prüfbereich:

1.1 Beschreibung des druckbeaufschlagten Bereiches:
 Schmielkörper und 2xV-Sammler mit 2x DN25 Stutzen und 27x Druckanschlüssen 6x1

2. Prüfvorschrift

Spezifikation: AD 2000 Sonstige:

3. Prüfdaten für Überdrucktest:

Prüffaktor F_p: 1,1
 Prüfdruck P_p[bar]: 6,2
 Prüftemperatur T_p[°C]: RT
 Tag der Prüfung: 10.11.2005

6. Bemerkungen/Abweichungen/Skizze:

Druckprüfung: Behälter mit Anschlußstutzen 100% in transparentem Wassertank untergetaucht mit Manometerüberwachung. (Einbauposition mit 2x DN 20 Stutzen vertikal nach oben)
 7. Prüfbefunde:
 - geringe Gasblasenbildung an Swagelocküberwurfmutter Pos.1+2 feststellbar.
 - Druckanzeige blieb oberhalb 6,2bar beständig. Keine Leckagen an Schweißnähten feststellbar.

.....FKZ-IKET, den 10.11.2005..... entfällt.....
 Ort, Datum
J.Rey.....
 Name (leserlich), Unterschrift (Prüfer) ggljs. Name (leserlich), Unterschrift (Betreiber)